GM-CSF differentiation of human monocytes stabilizes macrophage state via oxidative signaling

Christopher Y Itoh[1,2,3], Cal Gunnarsson[1,2], Gregory H Babunovic[2.3], Armel Nibasumba[2,3], Ngomu Akeem Akilimali[1,2], Marc H Wadsworth III[2,4,5], Travis K Hughes[2,4,5], Sydney L Solomon[1,2], Brian Hie[2,6], Bonnie Berger[6,7], Alex K Shalek[2,4,5,8], Sarah M Fortune[2,3], Bryan D Bryson[1,2]

1 Department of Biological Engineering, Massachusetts Institute of Technology, Cambridge, MA
2 Ragon Institute of MGH, MIT, and Harvard, Cambridge MA
3 Department of Immunology and Infectious Diseases, Harvard TH Chan School of Public Health, Boston MA
4 Department of Chemistry, Massachusetts Institute of Technology, Cambridge, MA
5 Institute for Medical Engineering and Science, Massachusetts Institute of Technology, Cambridge, MA
6 Computer Science and Artificial Intelligence Laboratory, Massachusetts Institute of Technology, Cambridge, MA
7 Department of Mathematics, Massachusetts Institute of Technology, Cambridge, MA
8 Koch Institute for Integrative Cancer Research, Massachusetts Institute of Technology, Cambridge, MA

Correspondence to: bryand@mit.edu (BDB)

Abstract

Macrophages are central mediators of immunity that integrate diverse signals derived from differentiation cues, tissue location, and disease. Controlling macrophage state and function is an appealing therapeutic objective across many diseases including cancer, atherosclerosis, and tuberculosis. Despite the growing appreciation for the *in vivo* complexity of macrophage state, existing *in vitro* models of human monocyte-derived macrophages have used a limited number of individual perturbations to explore the complex phenotypic space that macrophages can occupy. Here, we leverage a tiered differentiation, activation, and stimulation strategy to generate libraries of *in vitro* monocyte-derived macrophages and examine the *in vitro* state space of macrophage function using high-dimensional technologies. Our tiered experimental approach further revealed a striking relationship between GM-CSF differentiation and IL-10 production. Cells that were differentiated with GM-CSF produced very low or undetectable levels of IL-10 independent of activation or stimulation condition. To nominate candidate regulators of this IL-10 response, we leverage unbiased single-cell mRNA sequencing to identify transcriptional networks associated with GM-CSF-derived cells. Using these data, we identify oxidative signaling pathways as upregulated in GM-CSF derived cells and demonstrate that scavenging of oxidative radicals can enhance IL-10 production in these cells. Collectively, these data underscore the complexity of monocyte-derived macrophage state over time and highlight a dominant role for GM-CSF in tuning macrophage inflammatory phenotype, metabolic state, and plasticity.

Introduction

Understanding how macrophages interpret diverse signal inputs to dictate their state and function is an actively evolving field. While previous nomenclature to describe macrophage state adopted an M1 or M2 naming convention to parallel elements of Th1 and Th2 immunity, new naming conventions integrate additional dimensions of macrophage diversity including differentiation or activation cytokine and signal duration (Murray et al., 2014). This naming convention recognizes that distinct cues can drive specific cytokine-associated programs in addition to generic inflammatory or anti-inflammatory programs that are conserved across diverse inputs. As we continue to identify additional cues that redirect macrophage function, it is important to understand how these signals reinforce existing macrophage states or perturb them. Due to this evolving nomenclature, determining macrophage state using standard tools such as flow cytometry with canonical macrophage markers remains challenging as these markers are often expressed independent of macrophage state.

Recent murine studies highlight the complex and exquisite trajectories monocytes traverse as they differentiate into tissue-resident macrophages. In fact, in many tissues, monocyte-derived macrophages serve as the dominant contributor to the steady-state macrophage pool (Liu et al., 2019). These *in vivo* studies have been utilized to highlight features of macrophage plasticity and identify the signals that drive tissue-resident macrophage identity. For example, Lavin and colleagues demonstrated that tissue-resident macrophages can be transferred to new tissues and adopt features of the new microenvironment (Lavin et al., 2014). They demonstrated that peritoneal macrophages could be transferred intratracheally to the alveolar cavity of recipient mice and adopt features of the alveolar macrophages as evidenced by transcriptional profiling. These studies and countless others have been utilized to demonstrate features of macrophage phenotypic plasticity.

In contrast to the study of experimentally available murine tissue-resident macrophages, studies of human macrophages rely mostly on monocyte-derived macrophages differentiated from peripheral blood mononuclear cells of human donors. To differentiate these monocytes into macrophages, common protocols supplement culture media with either macrophage colony-stimulating factor (M-CSF) or granulocyte macrophage colony-stimulating factor (GM-CSF). Sander and colleagues utilized transcriptional profiling to demonstrate that human monocytes differentiated with M-CSF or GM-CSF resembled macrophages isolated directly from human ascites thus underscoring their experimental utility (Sander et al., 2017). Additionally, the authors demonstrated that monocytes integrate simultaneous signals from IL-4 and GM-CSF distinguishing them from monocytes differentiated with GM-CSF alone and suggest that varying the exposure time of IL-4 tunes the functional identity of the cells. Taken together, these previous studies highlight the complexity of macrophage behavior and their modes of signal integration.

To build upon these previous studies and examine how signal identity and duration influence human macrophage functional state, we established an *in vitro* experimental

platform to create libraries of monocyte-derived macrophages. Using a combination of flow cytometry, cytokine release assays, and single-cell RNA sequencing (scRNAseq), we demonstrate that GM-CSF differentiation of monocytes abolishes the capacity of these cells to produce IL-10 in response to TLR ligands. Moreover, we were unable to identify a cytokine or small molecule that was capable of restoring IL-10 production in these cells following differentiation. This finding provides an important update to the long-held model of macrophage plasticity. Using scRNAseq, we overcome existing challenges in macrophage characterization and identify novel markers of macrophage state that permit discrimination of macrophages on the basis of differentiation cytokine. We further leverage these scRNAseq results and nominate oxidative signaling as a driver of reduced IL-10 production in macrophages differentiated by GM-CSF which we then confirmed in our *in vitro* system. Taken together, these data emphasize the complexity of macrophage functional properties and suggest a dominant role for GM-CSF in modulating macrophage state.

Results:

Generation of libraries of *in vitro* monocyte-derived macrophages provides flexible platform for interrogating macrophage state and function

Human monocytes differentiated with M-CSF or GM-CSF are widely used as *in vitro* models for studying macrophage behavior (Lacey et al., 2012; Sander et al., 2017; Xue et al., 2014). To examine the contribution of these diverse axes, we generated libraries of *in vitro* monocyte-derived macrophages from CD14+ monocytes isolated from healthy human donors using a systematic framework for perturbation and characterization. CD14+ monocytes were first differentiated for 3 days with either GM-CSF or M-CSF to generate MO-GMCSF or MO-MCSF. To generate additional diversity in our *in vitro* cultures, on day 3 of differentiation, we supplemented our differentiation media with an additional activation stimulus (vehicle, LPS, IFN-γ, IL-4, IL-6, and IL-10) ultimately generating a total of 12 macrophage populations (**Figure 1A**) (Roussel et al., 2017).

We first utilized flow cytometry to characterize macrophage state by selecting commonly used macrophage surface markers from previous studies (Roussel et al., 2017). We compared surface expression of CD32, CD36, CD64, CD86, CD206, CD274, and HLA-DR focusing first on the differences in MO-MCSF and MO-GMCSF libraries separately. We used two metrics to characterize surface expression of these markers across our samples: (1) percentage of cells expressing any given marker relative to an isotype control and (2) the mean fluorescence intensity (MFI) of the surface markers. We sought to examine if any of the markers in our panel demonstrated digital expression among the macrophages generated in our *in vitro* libraries. In contrast to lymphocytes where several markers exist to distinguish subpopulations using a binary gating strategy, none of the macrophage markers used in this panel were capable of discriminating between the different macrophage populations (**Figure 1B, Supplemental Figure 1)** (DuPage and Bluestone, 2016; Murray et al., 2014)**.** As previously observed by others, our results displayed differences in the level of expression of various markers across all macrophage types (**Figure 1C, Supplemental Figure 2**) (Schulz et al., 2019). Specifically, we

observed CD274 consistently upregulated in cells stimulated with IFN-γ or LPS in both MO-MCSF and MO-GMCSF cells. **(Figure 1D (MO-MCSF), Supplemental Figure 3 (MO-GMCSF))**.

As a complementary approach to flow cytometry, we next characterized our macrophage library by examining cytokine release in response to purified TLR ligands. We initially conducted a multiplex cytokine screen focusing on the differences between MO-MCSF and MO-GMCSF in response to lipopolysaccharide (LPS), a TLR4 agonist and Pam3CSK4 (PAM), a TLR1/2 agonist, for 24 hours prior to cytokine analysis. We measured the release of several cytokines, including IL-1β, IL-6, and IL-10. Comparing MO-MCSF and MO-GMCSF cells, we observed a marked reduction in the production of IL-10 and CCL-2 in MO-GMCSF cells in response to both TLR ligands, consistent with previous reports comparing these cells (**Figure 1E**) (Lacey et al., 2012; Sander et al., 2017). We next extended these measurements to all twelve populations of MO-MCSF and MO-GMCSF cells. We focused on the production of TNFα, IL-6, and IL-10 given the dynamic range of their response to TLR stimulation. By enzyme-linked immunosorbent assay (ELISA), we were able to validate our observation of decreased production of IL-10 in GM-CSF derived cells. Notably, we observed levels of IL-10 production that were near or below the ELISA limit of detection across all MO-GMCSF cells independent of TLR stimulation or activation cue (**Figure 1F**). This was in contrast to M-CSF derived macrophages which retained their ability to produce IL-10. MO-GMCSF cells, despite lacking an IL-10 response, retained their ability to respond to TLR ligands and produce cytokines as indicated by production of TNFα (**Figure 1G**). We sought to recapitulate these findings using intracellular cytokine staining; however, we were unable to find a antibody clone that demonstrated robust differences between unstimulated and stimulated MO-MCSF cells (**Supplemental Figure 4**).

Since our cytokine secretion results pointed to an altered IL-10 signaling network in MO-GMCSF cells, we next sought to determine if MO-GMCSF cells were muted in both their IL-10 production and responsiveness or production alone. To assess the capacity of MO-GMCSF cells to respond to IL-10, we monitored the phosphorylation status of STAT3, a well-characterized protein downstream of IL10R, following stimulation with IL-10 (Niemand et al., 2003). We observed a dose-dependent increase in phosphorylated STAT3 relative to total STAT3 in MO-GMCSF cells indicating that GM-CSF differentiation does not abrogate IL10R signaling (**Figure 1H)**. Collectively, these data demonstrate how macrophage differentiation cues can precisely fine-tune macrophage state and illustrate the utility of diverse modalities to characterize macrophage phenotypes.

scRNAseq reveals novel markers of the MO-GMCSF state

Given the phenotypic differences observed between MO-MCSF and MO-GMCSF cells, we employed scRNAseq to identify additional markers capable of distinguishing between these two macrophage states. To robustly interrogate the transcriptomes of thousands of cells we used Seq-Well, a nanowell platform for high-throughput scRNAseq (Gierahn et al., 2017). This produced 1,742 high-quality MO-GMCSF and 4,803 high-quality MO-MCSF cellular transcriptomes from 2 donors (**Supplementary Figure 5**). We first

185 examined the expression of canonical markers of macrophage state to characterize their
186 ability to discriminate between MO-MCSF and MO-GMCSF cells. A subset of canonical
187 marker genes achieved statistically significant differential expression (CD68, CD86,
188 MRC1 (CD206); however, the magnitude of their transcriptional difference was minimal
189 (**Figure 2A**, **Supplementary Table 1**). Other canonical markers either displayed no
190 significant differences or had low capture rates. We next examined the expression of all
191 genes measured by scRNAseq. Using a Wilcoxon rank sums test, we identified 178
192 significantly upregulated and 137 significantly downregulated genes in MO-GMCSF cells
193 relative to MO-MCSF cells (**Figure 2B**). We identified several novel marker genes of MO-
194 MCSF and MO-GMCSF cells. We identified CHI3L1 and MGLL as markers of MO-MCSF
195 and TXN and ALOX5AP as markers of MO-GMCSF (**Figure 2C**). These genes included
196 CHI3L1 and MGLL as markers of MO-MCSF and TXN and ALOX5AP as markers of MO-
197 GMCSF. To gain an unbiased view of the transcriptional programs differentially active in
198 MO-MCSF and MO-GMCSF cells, we next identified Gene Ontology Molecular Function
199 (GO MF) terms enriched in the set of marker genes for each state. This analysis revealed
200 MO-GMCSF cells were marked by transcriptional programs related to redox signaling, as
201 well as antigen presentation (**Figure 2D, Supplementary Table 2**).
202
203 Using scRNAseq, we found several novel markers that distinguished MO-MCSF and MO-
204 GMCSF cells. The gene encoding thioredoxin (*TXN*) was a robust marker of MO-GMCSF
205 cells by an AUC classifier (AUC = 0.85). Thioredoxin is an antioxidant that is involved in
206 many different signaling pathways via redox control (Lee et al., 2013). Previous studies
207 in human macrophage-like cell lines have demonstrated that thioredoxin is highly
208 expressed in response to the combination of LPS and IFN-γ, a well-characterized inducer
209 of an inflammatory phenotype (Plugis et al., 2018). Other studies have suggested that
210 MO-GMCSF cells may serve as another model of inflammatory macrophages (Fleetwood
211 et al., 2007; Hamilton, 2019). We hypothesized that the induction of thioredoxin may be
212 conserved in both MO-MCSF treated with LPS+IFN-γ and MO-GMCSF cells. Consistent
213 with the scRNAseq data and our hypothesis, thioredoxin protein was highly expressed in
214 MO-GMCSF, as well as M(LPS+IFN-γ), compared to MO-MCSF cells (**Fig 2E**). We next
215 sought to validate an additional marker of MO-GMCSF, 5-lipoxygenase accessory protein
216 (ALOX5AP), which is essential for the production of inflammatory lipids such as
217 prostaglandin E2. Again, consistent with our scRNAseq data, ALOX5AP was highly
218 expressed in MO-GMCSF cells relative to MO-MCSF cells; however, ALOX5AP was not
219 highly expressed in M(LPS+IFN-γ), suggesting distinct regulatory axes contributing to
220 expression of these marker genes (**Figure 2F**). These results are consistent with previous
221 work demonstrating altered expression of ALOX5AP and dichotomous production of
222 inflammatory and pro-resolving lipids (Werz et al., 2018). Further supporting our
223 scRNAseq results, we also observed enhanced expression of CD36 on MO-MCSF cells
224 and increased expression of CD206 on MO-GMCSF cells by flow cytometry (**Figure 2G,**
225 **Figure 2H**). Taken together, these results identify novel markers that can more definitively
226 characterize macrophage state and distinguish common transcriptional programs that are
227 active across macrophage culture systems.
228
229 **GM-CSF mediates a durable switch in IL-10 production**
230

231 We reasoned that the immunophenotyping analyses had provided us with markers that
232 we could leverage to interrogate phenotypic transitions between macrophage state.
233 Macrophages have long been described as cells that demonstrate exquisite phenotypic
234 plasticity; however, our IL-10 secretion results suggested that following GM-CSF
235 differentiation, several cytokines were unable to enhance TLR-mediated IL-10 production
236 to levels above the detection limit (Biswas and Mantovani, 2010; Liu et al., 2020; Locati
237 et al., 2020).
238
239 Using IL-10 production in response to TLR stimulation as a measure of macrophage state,
240 we sought to interrogate the stability of the MO-MCSF and MO-GMCSF phenotype. We
241 first sought to examine the expression of M-CSF and GM-CSF receptors on the surface
242 of MO-MCSF and MO-GMCSF cells reasoning that we might be able to utilize the
243 opposing cytokine to shift macrophage state. We performed flow cytometry on MO-MCSF
244 or MO-GMCSF cells following 6 days of differentiation. We detected surface expression
245 of GM-CSF (CD116) and M-CSF (CD115) receptors on the surface of MO-MCSF and
246 MO-GMCSF cells (**Figure 3A**). We next sought to examine how treatment of MO-MCSF
247 and MO-GMCSF cells with the opposing cytokine would modulate IL-10 production.
248 Monocytes were differentiated in the presence of M-CSF or GM-CSF for 6 days, washed,
249 and then cultured in media containing 50 ng/mL M-CSF, media containing 50 ng/mL GM-
250 CSF, or media alone for an additional 3 days. After this second phase of culture, cells
251 were washed and then stimulated with LPS for 24 hours prior to analysis of IL-10 secretion
252 (**Figure 3B**). As expected from our previous observations, MO-MCSF cells that received
253 no cytokine or M-CSF during the second media phase produced IL-10 in response to
254 LPS. In contrast, MO-MCSF cells treated with GM-CSF during the second media phase
255 produced less IL-10 in response to LPS (**Figure 3C**). Strikingly, MO-GMCSF cells
256 independent of their second media phase did not produce IL-10 at levels above the limit
257 of detection in response to LPS stimulation similar to our results observed with IFN-γ, IL-
258 4, IL-6, IL-10, and LPS.

259 While macrophages may encounter asynchronous stimuli as modeled by temporally
260 staggering the addition of cytokines, we reasoned that monocytes upon recruitment to
261 tissues may simultaneously encounter combinations of cytokines such as M-CSF and
262 GM-CSF that may act synergistically to drive the functional state of the resulting
263 macrophages. We next sought to examine whether the monocyte response to GM-CSF
264 or M-CSF differentiation could be modeled as an additive response. To examine these
265 dynamics, we generated a matrix of combinations of M-CSF and GM-CSF ranging from
266 0 ng/mL to 50 ng/mL in ten-fold increments (**Figure 3D, Figure 3E**). Cytokines were
267 premixed and arrayed prior to the addition of monocytes to eliminate any temporal
268 asynchrony in cytokine exposure. Monocytes were differentiated for 6 days, washed, and
269 then stimulated with LPS. IL-10 production was monitored by ELISA. Monocytes cultured
270 for 6 days in the absence of exogenous cytokines on tissue-culture treated plasticware
271 did not survive. In the absence of GM-CSF, we observed a dose-dependent increase in
272 LPS-mediated IL-10 release as we increased the concentration of M-CSF in the
273 differentiation media. Holding the M-CSF concentration at 0 ng/mL, we observed no
274 increase in LPS-mediated IL-10 production as the concentration of GM-CSF increased.
275 Intriguingly, nearly all combinations of M-CSF and GM-CSF resulted in low or
276 undetectable levels of IL-10 in response to LPS suggesting a non-additive hypersensitivity

277 to GM-CSF in driving macrophage state as previously observed at the transcriptional level
278 (Lacey et al., 2012). Taken together, these data highlight the potency of GM-CSF in
279 modulating macrophage state and underscore the importance of understanding the
280 additive and non-additive gene and protein expression relationships in myeloid cells.
281
282 **Disruption of elements of the canonical GM-CSF signaling network does not**
283 **enhance IL-10 production in MO-GMCSF cells but scavenging of ROS does.**
284
285 Our tiered macrophage differentiation strategy did not identify a cytokine capable of
286 restoring IL-10 production in MO-GMCSF cells. As an alternative strategy to
287 mechanistically dissect the drivers of muted IL-10 production in MO-GMCSF cells, we
288 turned to previously established models for modifying either macrophage phenotypic
289 stability or IL-10 production.
290
291 Previous studies in murine and human macrophages have demonstrated that
292 macrophages adopt semi-stable phenotypes as demonstrated by surface marker and
293 marker gene expression (Van den Bossche et al., 2016). In these studies, the authors
294 implicate mitochondrial dysfunction mediated by inducible nitric oxide synthase (iNOS) as
295 a driver of limited M1 to M2 repolarization in murine macrophages. We sought to test the
296 hypothesis that iNOS may play a role in the limited plasticity observed in MO-GMCSF
297 cells recognizing that expression of iNOS in human macrophages has been widely
298 debated (Bogdan, 2001; Schneemann and Schoedon, 2002). Nevertheless, we sought to
299 reproduce the experimental model employed previously to examine functional stability in
300 MO-GMCSF macrophages. Human monocytes were pre-treated with 1400W, an iNOS
301 inhibitor, or DMSO for one hour prior to the addition of M-CSF or GM-CSF. After 6 days,
302 the cells were washed and stimulated with LPS. Production of IL-10 was observed in all
303 MO-MCSF cells; however, IL-10 remained undetectable in MO-GMCSF cells across all
304 conditions (**Figure 4A**).
305
306 Salt inducible kinase (SIK) inhibitors were previously identified as potentiators of IL-10
307 production in macrophages following their differentiation into macrophages (Lombardi et
308 al., 2016; MacKenzie et al., 2013). We examined the capacity of salt inducible kinase
309 inhibitor, HG-9-91-01, to enhance IL-10 production in MO-MCSF and MO-GMCSF cells.
310 MO-MCSF and MO-GMCSF cells were incubated with HG-9-91-01 for 2 hours prior to
311 the addition of LPS; however, we observed no increase in the production of IL-10 in SIK-
312 inhibitor treated cells relative to the vehicle control (**Figure 4B**). To test the hypothesis
313 that the absence of robust IL-10 production in MO-GMCSF cells was mediated by the
314 activity of epigenetic regulators, we next examined the contribution of Class I and Class
315 II histone deacetylases by pre-treating the cells with trichostatin A (TSA), an inhibitor of
316 these enzymes, prior to the addition of GM-CSF. Pre-treatment with 100 nM TSA had no
317 impact on the capacity of MO-GMCSF cells to produce IL-10 (**Figure 4C**). In parallel, we
318 sought to interrogate the effects of M-CSF and GM-CSF treatment on chromatin
319 accessibility through the lens of ATAC-sequencing with a specific focus on the IL-10
320 locus. IL-10 did not achieve a statistically significant p-value after Bonferroni hypothesis
321 correction (**Supplemental Table 3**).
322

Interfering with previously described networks involved in IL-10 production or phenotypic stability in macrophages had minimal impact in enhancing IL-10 production in MO-GMCSF cells.

We next sought to review our unbiased transcriptomic data for additional insight and hypotheses for programs that we could perturb in MO-GMCSF cells to restore IL-10 production. In MO-GMCSF cells, we observed statistically significant enrichment of pathways associated with oxidoreductase signaling including TXN, SOD2, and GLRX (**Figure 4D**). We next sought to examine the contribution of oxidative signaling in MO-GMCSF cell function by first pre-treating monocytes with N-acetylcysteine (NAC) for one hour prior to the addition of M-CSF or GM-CSF. After 6 days, the cells were washed and stimulated with LPS. As expected, production of IL-10 was observed in all MO-MCSF cells. Consistent with a model whereby oxidative signaling contributes to the suppression of IL-10 release in MO-GMCSF cells, pre-treatment of monocytes with NAC prior to the addition of differentiation cytokines mediated an increase in IL-10 release following LPS treatment, though not to levels of MO-MCSF cells (**Figure 4E**). Together, these data demonstrate the utility of unbiased approaches to augment hypothesis generation as well as underscore the contribution of immunometabolic circuits to macrophage state.

Discussion

Macrophage states, mostly studied through the lens of M1 and M2 activation, have been studied extensively both *in vivo* and *in vitro.* Many models have been proposed to describe the mechanisms that underlie macrophage state in a diverse array of settings (Lawrence and Natoli, 2011; Murray, 2017). Traditionally, macrophages have long been considered to be plastic cells that can polarize to distinct states as needed. However, challenges exist when determining macrophage state and examining phenotypic transitions in tissues in a cell type such as primary human macrophages. Unlike lymphocytes, few, if any, robust binary markers exist for cell state determination in primary human macrophages. Here, we studied a widely utilized model of human macrophages using high-resolution tools to define novel markers of cell state and examine macrophage functional stability. Using our systematic approach to examine macrophage state, we show that MO-GMCSF cells adopt a stable phenotype with respect to IL-10 production and that this phenotype can be disrupted by the addition of scavengers of reactive oxygen species.

We show that conventional surface markers are of limited utility to discern macrophage state using a binary gating strategy. These results are consistent with countless previous studies that utilize analog differences in surface protein expression instead of digital expression as done with lymphocytes (Becher et al., 2014; Roussel et al., 2017; Schulz et al., 2019). Cytokine profiling in response to TLR ligands helped discriminate LPS-tolerized macrophages in both MO-MCSF and MO-GMCSF states. Moreover, cytokine profiling aided in discriminating MO-MCSF and MO-GMCSF cells through the lens of IL-10 production, consistent with previous studies of MO-MCSF and MO-GMCSF cells (Lacey et al., 2012; Sander et al., 2017). Here, our work extends upon these previous

368 studies by examining the temporal dimension of macrophage state and reveals the
369 striking stability in macrophage state that can be achieved.
370
371 To address challenges in characterizing macrophage state using protein expression, we
372 conducted scRNAseq of MO-MCSF and MO-GMCSF cells and identified numerous novel
373 markers of macrophage state. Namely, in MO-GMCSF cells, we identified strong
374 enrichment of pathways associated with oxidative signaling consistent with emerging
375 models relating metabolism in driving macrophage state (Cameron et al., 2019; West et
376 al., 2011). We speculate that this interplay between oxidative signaling and metabolic
377 state influence a multitude of macrophage functions, such as bacterial clearance and
378 atherosclerosis, *in vivo* (Di Gioia et al., 2020; Huang et al., 2018; Wang et al., 2020). We
379 identified and validated several novel markers of macrophage state. We also highlight
380 shared programs that are active across multiple models of inflammatory macrophages
381 such as thioredoxin signaling, as well as programs such as ALOX5AP that are specific to
382 differentiation cue. Previous studies in human macrophages are consistent with our
383 unbiased study of macrophage gene expression. Studies by Werz and colleagues
384 similarly observed digital expression of ALOX5AP in MO-GMCSF cells and demonstrate
385 that this digital protein expression is correlated with digital production of the inflammatory
386 lipid PGE2 (Werz et al., 2018). Taken together, these data identify novel markers of
387 macrophage state as well as regulatory axes that should be considered when selecting
388 *in vitro* culture models. PGE2 has been previously demonstrated to modulate
389 macrophage state through the lens of metabolic function and cytokine release highlighting
390 a critical role for this lipid in immunoregulation (MacKenzie et al., 2013; Sanin et al., 2018).
391 It is appealing to hypothesize that high levels of PGE2 production and low IL-10
392 production may contribute to amplification of an inflammatory macrophage state.
393
394 Using IL-10 release as a tool to interrogate functional stability of MO-MCSF and MO-
395 GMCSF cells. Surprisingly, we observed that MO-MCSF cells retained functional
396 plasticity with respect to IL-10 production while MO-GMCSF cells did not. Previous
397 studies in primary human macrophages demonstrate that classical M(LPS+IFN-γ)
398 macrophages do not upregulate CD206 and CD200R markers upon treatment with IL-4
399 whereas M-CSF macrophages do upregulate CD206 and CD200R when treated with IL-
400 4 (Van den Bossche et al., 2016). IL-10 production has traditionally been associated with
401 anti-inflammatory macrophage states. Our *in vitro* results demonstrate a shared property
402 among inflammatory macrophages where limited phenotypic transitions from
403 inflammatory to anti-inflammatory states are possible. Previous studies in M(LPS+IFN-γ)
404 human macrophages did not identify a strategy to reverse the inflammatory state. Here,
405 using an unbiased systems-level analysis, we identified oxidative signaling as a driver of
406 IL-10 suppression. Our results demonstrating an association between GM-CSF signaling
407 and reactive oxygen species is consistent with several other studies demonstrating a role
408 for GM-CSF in modulating ROS production in diverse myeloid cell types (Kasahara et al.,
409 2016; Spath et al., 2017; Subramanian Vignesh et al., 2013). Our protein expression
410 analysis revealed that thioredoxin was highly expressed in both MO-GMCSF and
411 M(LPS+IFN-γ) cells suggesting a potentially conserved mechanism whereby oxidative
412 signaling contributes to inflammatory macrophage phenotypic stability. Previous work has
413 highlighted the transcriptional regulator BHLHE40 as an essential repressor of IL-10

414 production in murine cells treated with GM-CSF; however, regulation of BHLHE40
415 expression in M(LPS+IFN-γ) has not been explored (Huynh et al., 2018). Upregulation of
416 BHLHE40 has been observed in response to DNA damaging agents, and recent studies
417 demonstrate that DNA damage mediated by reactive oxygen species is observed in
418 murine macrophages following the addition of inflammatory agents such as LPS and IFN-
419 γ (Cameron et al., 2019; Kim et al., 2014). Examining the regulation of BHLHE40
420 expression and the contribution of BHLHE40 in inflammatory macrophage stability should
421 be the subject of future inquiry.
422
423 While many *in vitro* macrophage models focus on driving a particular state in a digital
424 fashion providing a single cytokine in isolation, here, we began to investigate the role of
425 combinations of cytokines in mediating cell state. Again, even when M-CSF is provided
426 in excess, we observed that GM-CSF is incredibly potent in mediating IL-10 suppression.
427 In tissues where GM-CSF is constitutively present like the lungs, it is highly plausible that
428 GM-CSF may play a dominant role in modulating macrophage function independent of
429 ontogeny. In fact, previous studies of isolated murine alveolar macrophages show
430 undetectable or very low levels of IL-10 production in response to TLR ligands (Sajti et
431 al., 2020; Salez et al., 2000). These data raise the possibility that MO-GMCSF cells may
432 provide a functionally similar macrophage to those isolated from tissues consistent with
433 transcriptional analyses performed by Sander; however, additional functional studies are
434 necessary to more fully characterize axes of *in vitro* and tissue-resident macrophage
435 state. These data suggest that complex immune environments may contain dominant
436 soluble mediators of cell state, similar to how GM-CSF drives a low-IL-10 producing state
437 even at low concentrations. How these relationships scale for other cytokine pairs and
438 other responses has been partially investigated in the past; here we build on the
439 experimental designs employed in those studies with a cellular reprogramming model
440 involving staggered addition of cytokines or TLR ligands and suggest future work to
441 explore combinatorial signal perception and gene expression manifolds more
442 exhaustively in macrophages (Natarajan et al., 2006; Xue et al., 2014).
443
444 Since human monocyte-derived macrophages have limited to non-existent replicative
445 capacity, leveraging the markers identified in our study may allow recovery of cellular
446 history in a manner akin to fate-mapping experiments conducted in genetically
447 engineered mice. Future studies should further define the relationship between signal
448 inputs and the expression of markers identified in our study. We found that GM-CSF was
449 a driver of ALOX5AP expression; however, it is not known if there are other cytokines that
450 induce ALOX5AP expression. Similarly, we identified TXN as a marker of MO-GMCSF
451 cells as well as MO(LPS+IFN-γ) cells. Shared expression of TXN in MO(LPS+IFN-γ) and
452 MO-GMCSF cells suggests a shared response network, possibly oxidative signaling, and
453 may serve as an equally valuable marker to inform metabolic history of immune cells.
454 Lastly, as we continue to decipher the relationship between marker expression and
455 cytokine stimulation, it will be essential to understand the relationship between signal
456 duration and magnitude and marker expression to fully exploit the potential of these novel
457 markers.
458

In conclusion, our study demonstrates the phenotypic stability of MO-GMCSF cells by exploring the temporal dimension of macrophage state. Here, we demonstrate using a combination of immune profiling assays with scRNAseq that oxidative signaling contributes to limited IL-10 release in human macrophages. For future work, we propose deeper study of metabolic and oxidative signaling in both MO-GMCSF and other models of inflammatory macrophages to identify shared mechanisms of phenotypic stability.

Methods

PBMC Isolation and Monocyte Differentiation

Deidentified buffy coats from healthy human donors were obtained from Massachusetts General Hospital. PBMCs were isolated from buffy coats by density-based centrifugation using Ficoll (GE Healthcare). CD14+ monocytes were isolated from PBMCs using a CD14 positive-selection kit (Stemcell). Isolated monocytes were differentiated to MO-MCSF or MO-GMCSF in RPMI 1640 (ThermoFisher Scientific) supplemented with 10% heat-inactivated FBS (ThermoFisher Scientific), 1% HEPES, and 1% L-glutamine. Media was further supplemented with either 50 ng/mL M-CSF or 50 ng/mL GM-CSF unless otherwise specified (Biolegend, MCSF: 572902 and GM-CSF: 574802). Monocytes were cultured on low-adhesion tissue culture plates (Corning) for 6 days. Where specified, additional polarization stimuli were added on day 4 (10 ng/mL IFN-γ, 10 ng/mL IL-4, 10 ng/mL IL-6, 10 ng/mL IL-10, and 10 ng/mL LPS) for a total of 6 days in culture. For 6 well dishes, cells were seeded at a density of 0.5e6 cells/mL. For 12- and 96-well dishes, cells were seeded at a density of 0.25e6 cells/mL.

Surface Epitope Staining and Flow Cytometry

Macrophages were detached from low-adhesion tissue culture plates using pre-warmed 1X PBS (Ca2+ and Mg2+ free) (Corning, 21-040-CV) supplemented with 2mM EDTA. Detached macrophages were counted, pelleted at 500xg, and blocked using Human TruStain FcX (Biolegend: 422301) at 2x for 5 min at room temperature. Cells were then stained directly using a pre-mixed antibody panel cocktail for 15 min in the dark at 4° C. Cells were then washed twice with FACS buffer (1X Ca2+ and Mg2+ free PBS, 2% heat-inactivated FBS, and 1mM EDTA) prior to fixation in 2% paraformaldehyde for 15 minutes at room temperature. Following fixation, cells were washed twice with FACS buffer and then analyzed by flow cytometry.

Antibody panels are as follows:
Panel 1: CD11b-BV421 (Biolegend, 301323), CD32-PECy7 (Biolegend, 303213), CD36-APC (Biolegend, 336207), HLA-DR-BV510 (Biolegend, 307645)
Panel 2: CD11b-BV421 (Biolegend, 301323), CD274-PE (Biolegend, 329705), CD86-APC (Biolegend, 305411), CD64-BV510 (Biolegend, 305027)

Additional antibodies utilized in this study included CD36-PE (Biolegend, 336205), CD206-PE (Biolegend, 321105), CD123 (Biolegend, 306005), CD125 (R&D Systems, FAB253P), CD115-BV421 (Biolegend, 347321), CD116-PE (Biolegend, 305908).

505
506 Samples were analyzed on a BD LSR Fortessa.
507
508 **Intracellular Cytokine Staining and Flow Cytometry**
509
510 MO-MCSF cells were simultaneously treated with Brefeldin A (Biolegend, 420601) and
511 stimulated with 100 ng/mL LPS for 12 hours. After this incubation, cells were detached
512 from low-adhesion tissue culture plates using pre-warmed 1X PBS (Ca2+ and Mg2+ free)
513 (Corning, 21-040-CV) supplemented with 2mM EDTA. Detached macrophages were
514 counted, pelleted at 500xg, and resuspended in Fixation Buffer (Biolegend, 420801) and
515 allowed to fix for 20 minutes at room temperature in the dark. Following fixation, cells
516 were pelleted at 500xg and resuspended in Intracellular Staining Perm Wash Buffer
517 (Biolegend, 421002). Three total washes in Intracellular Staining Perm Wash Buffer were
518 performed. Following permeabilization, cells were pelleted for 5 minutes at 500xg and
519 resuspended in 50 µL Intracellular Staining Perm Wash Buffer supplemented with 5 µL
520 of TruStain FcX (Biolegend, 422302) for 10 minutes at room temperature. Then, 50 µL
521 Intracellular Staining Perm Wash Buffer supplemented with 5 µL of IL-10-BV421 antibody
522 (Biolegend, 501421) was added for an additional 20 minutes at room temperature.
523 Following antibody incubation, cells were pelleted for 5 minutes at 500xg and washed
524 twice with Intracellular Staining Perm Wash Buffer prior to resuspension in FACS buffer
525 (1X Ca2+ and Mg2+ free PBS, 2% heat inactivated FBS, and 1mM EDTA) prior to
526 analysis on a BD LSR Fortessa.
527
528 **Luminex**
529
530 MO-GMCSF or MO-MCSF cells were treated for 16 hours with either 100 ng/mL LPS or
531 100 ng/mL Pam3CSK4 prior to analysis of cytokine release. Multiplexed cytokine
532 measurements on macrophage cell culture supernatants were performed using a custom
533 Bio-Plex Express Human Cytokine kit (Bio-Rad 17004073) according to manufacturer's
534 instructions, using a Bio-Plex 3D Suspension Array System (Bio-Rad). Measured
535 cytokines included IL-6, IFN-γ, GM-CSF, TNFα, IL-1β, IP-10 (CXCL10), MCP-1 (CCL-2),
536 IL-8, IL-10, and IL-12p70. Supernatants were stored at -80°C until analysis.
537
538 **Enzyme-linked Immunosorbent Assays (ELISA)**
539
540 0.25e6 cells were plated per well of a 12 well dish for cytokine release assays. Cells were
541 stimulated with either 100 ng/mL LPS or 100 ng/mL Pam3Csk4 for 16 hours.
542 Supernatants were analyzed fresh or stored at -80°C until analysis. Cytokine release was
543 measured by ELISA using TNFα, IL-6, and IL-10 ELISA kits (Biolegend: TNFα 430201,
544 IL-6 430501, and IL-10 430601).
545
546 **Single Cell RNA Sequencing**
547
548 We performed SeqWell analysis as previously described (Gierahn et al., 2017). Briefly,
549 beads were loaded into the PDMS array followed by subsequent addition of ~12,000 cells.

After periodic gentle rocking and washing, a polycarbonate membrane was attached to the array surface.

After membrane attachment, the array was transferred to a dish containing cell lysis buffer. After lysis, buffer was exchanged for hybridization buffer to enable RNA hybridization to barcoded beads. Beads were removed from microwell arrays by scraping the array with a microscope slide.

Recovered beads were transferred to a 1.5 mL tube and reverse transcription was performed using Maxima H- reverse transcriptase (Invitrogen). Beads were then treated with ExoI to digest unoccupied primer sites (NEB).

cDNA was amplified and the pooled PCR library was purified, and tagmentation was subsequently performed. Libraries were sequenced on an Illumina NextSeq500. 20 bases were allocated (12 bp cell barcode and 8 bp UMI) for Read 1, which was primed using Custom Read 1 Primer.

Transcriptome Alignment

Read alignment was performed as in described previously (Macosko et al., 2015). Briefly, for each NextSeq sequencing run, raw sequencing data was converted to FASTQ files using bcl2fastq2 that were demultiplexed by Nextera N700 indices corresponding to individual samples. Reads were first aligned to HgRC19 and individual reads were tagged according to the 12-bp barcode sequence and the 8-bp UMI contained in read 1 of each fragment. Following alignment reads were binned and collapsed onto 12-bp cell barcodes that correspond to individual beads using DropSeq tools (http://mccarrolllab.com/dropseq/). Barcodes were collapsed with a single-base error tolerance (Hamming distance =1) with additional provision for single insertions or deletions. An identical collapsing scheme (Hamming distance = 1) was then applied to unique molecular identifiers to obtain quantitative counts of individual mRNA molecules.

Single Cell RNAseq Data Pre-Processing

We identified a total of 1,742 good-quality GM-CSF-macrophages (donor 1: 399, donor 2: 1,343) and 4,803 good-quality M-CSF-treated cells (donor 1: 1,941, donor 2: 2,862) with total transcripts >2,500 and <75,000 and mitochondrial read percentage less than 20%. After filtering based on quality control metrics, raw count matrices were normalized by library size. For each cell, UMI-collapsed gene expression counts were divided by total transcript counts for that cell, multiplied by a scale factor of 10,000, then natural logarithm-normalized using Seurat v3.0.2. Log-transformed expression levels were standard scaled using Seurat's ScaleData function. During scaling, technical covariates (percentage mitochondrial reads and number of UMIs) were regressed out using a generalized linear model, as implemented in Seurat, and the residuals of the generalized linear model were used as 'corrected' gene expression values for downstream scaling.

Differential Expression Analysis

Differential gene expression between MO-MCSF and MO-GMCSF macrophages was assessed by Wilcoxon and AUC tests using Seurat's FindMarkers function and log-transformed expression levels [ln(TPM+1)]. Genes with absolute log2 fold change > 0.25 and Bonferroni-corrected p-values < 0.05 were considered differentially expressed genes (DEGs). DEGs with AUC < 0.7 or AUC > 0.3 were selected as markers of MO-GMCSF and MO-MCSF macrophages, respectively. Differential expression analyses were conducted on individual donors separately, as well as on all cells together.

Gene Ontology Enrichment Analysis

Gene symbols were mapped to Entrez gene ids using org.Hs.eg.db annotations. GO enrichment was analyzed by hypergeometric test using the clusterProfiler package's enrichGO function against a background set of genes captured in all sequencing runs with > 100 total counts across runs. GO terms with Benjamini-Hochberg-correct p-values < 0.05 were considered significantly enriched. Significant GO terms were collapsed into representative GO terms using clusterProfiler's simplify function and a similarity threshold of 0.7.

Data availability

All RNA-seq data are available in GEO under accession number XXXX. Code needed to complete the RNA-seq analysis can be found on github.com/cgunnars/mcsf-gmcsf-sc

Western Blotting

Macrophages were lysed using RIPA buffer with Proteinase Inhibitor. Protein concentration was estimated using a BCA assay. 15ug of protein were loaded per sample in a Bolt 4-12% Bis-Tris Plus Gel. PageRuler Plus was used as a molecular weight ladder. The gel was transferred to a nitrocellulose membrane using the iBlot 2 dry blotting system (Invitrogen). Membranes were blocked for 1 hour using Odyssey blocking buffer at room temperature. Membranes were next incubated in primary antibody shaking overnight at 4C. TRX (Santa Cruz, sc-166393), β-actin (Biolegend, Poly6221), ALOX5AP (GeneTex, GTX106689), and β-actin (Santa Cruz, sc-47778) were diluted with TRIS buffered saline containing Tween-20 (TBST). After incubation with the primary antibody, membranes were washed three times with TBST and then incubated with a fluorescent secondary antibody (LiCor IRDye 680 or LiCor IRDye 800) at a dilution of 1:10,000 in TBST for 1 hour. The membranes were then washed three times with TBST. The western blots were imaged by Odyssey CLx.

STAT3 Phosphorylation Analysis

MO-MCSF or MO-GMCSF cells were washed once with PBS following 6 days of differentiation, and then stimulated with media containing vehicle or media containing 10 or 50 ng/mL IL-10 for 15 minutes. Following incubation with IL-10, cells were washed once with cold PBS and lysed immediately on ice. Western blotting was performed as described above. Membranes were incubated with either a total STAT3 antibody (Cell

641 Signaling Technology, Clone: 79D7) or a phosphorylated STAT3 antibody (Cell Signaling
642 Technology, Clone: D3A7).
643
644 **Macrophage Durability Assay**
645
646 To evaluate the stability of TLR-mediated IL-10 release by macrophages, following 6 days
647 of differentiation with M-CSF or GM-CSF, MO-MCSF cells or MO-GMCSF cells were
648 washed with pre-warmed media without cytokines and then incubated with media
649 supplemented with 50 ng/mL M-CSF, 50 ng/mL GM-CSF or no cytokine. Following 3 days
650 of incubation, cells were washed with PBS and then stimulated with 100 ng/mL LPS for
651 16 hours prior to quantification of IL-10 release by ELISA.
652
653 **GM-CSF + M-CSF Checkerboard Assay**
654
655 For the GM-CSF/M-CSF checkerboard assay, a range of concentrations of GM-CSF and
656 M-CSF (0, 0.5 ng/mL, 5 ng/mL, and 50 ng/mL) were premixed in a pairwise fashion prior
657 to the addition of monocytes. Monocytes were then added to the individual wells to
658 commence differentiation. Monocytes were allowed to differentiate for 6 days. After 6
659 days, cells were washed twice with PBS and incubated with maintenance media with or
660 without 100 ng/mL LPS.
661
662 **GM-CSF and Drug Perturbation Experiments**
663
664 To evaluate the impact of inhibition of iNOS on IL-10 production in MO-MCSF and MO-
665 GMCSF cells, monocytes were pretreated with 1400W, an iNOS inhibitor, at a final
666 concentration of 100 μM for 1 hour prior to the addition of 50 ng/mL GM-CSF or 50 ng/mL
667 M-CSF. 1400W was dissolved in DMSO. After 6 days of differentiation, cells were washed
668 and then treated with 100 ng/mL LPS for 16 hours. Cytokine release was compared to
669 cells treated with DMSO alone (0.1% v/v final concentration). Supernatants were
670 analyzed fresh or stored at -80°C until analysis.
671
672 To evaluate the capacity of salt-inducible kinase inhibitor or PGE2 treatment on
673 production of IL-10 by MO-MCSF cells, cells were pre-treated with DMSO (0.1% v/v), 250
674 or 500 nM HG-9-91-01 (VWR, dissolved in DMSO, final concentration 0.1% v/v DMSO),
675 or 5 or 10 μM PGE2 (Santa Cruz Biotechnology) for two hours prior to treatment with
676 LPS. Without washing, cells were then treated with 100 ng/mL LPS for 16 hours prior to
677 analysis by ELISA.
678
679 To evaluate the impact of inhibiting class I and II histone deacetylases, monocytes were
680 pretreated with 100 nM trichostatin A (TSA, Sigma Aldrich). Monocytes were pre-treated
681 for 1 hour prior to the addition of 50 ng/mL GM-CSF or 50 ng/mL M-CSF to induce
682 differentiation. After 6 days of differentiation, cells were washed and then treated with 100
683 ng/mL LPS for 16 hours. Supernatants were analyzed fresh or stored at -80°C until
684 analysis.
685

686 To evaluate the impact of scavenging oxidative radicals prior to differentiation, monocytes
687 were pretreated with 5 mM N-acetylcysteine (NAC) which was dissolved directly in cell
688 culture media and filtered through 0.2 µm filter. Monocytes were pre-treated for 1 hour
689 prior to the addition of 50 ng/mL GM-CSF or 50 ng/mL M-CSF to induce differentiation.
690 After 6 days of differentiation, cells were washed and then treated with 100 ng/mL LPS
691 for 16 hours. Supernatants were analyzed fresh or stored at -80°C until analysis.
692
693 **ATAC Sequencing and Analysis**
694
695 MO-GMCSF and MO-MCSF cells were prepared for ATAC sequencing as previously
696 described (Buenrostro et al., 2015). Briefly, cells were detached and washed twice in PBS
697 and diluted to a final concentration of 1e6 cells/mL. 5,000 cells were then mixed with TD
698 buffer, 10% NP-40, 20x Illumina Tn5, and water. The reaction was allowed to proceed for
699 30 mins with shaking at 37°C with mixing. Transposed DNA is isolated using a PCR
700 purification kit (Qiagen) and eluted. 5 cycles of PCR were performed on the transposed
701 product with indexing primers and qPCR was performed on 5 µL of the PCR product to
702 identify the optimal number of total cycles for each sample. The remaining PCR mix was
703 stored on ice until the optimal number of additional cycles was identified. The amplified
704 PCR product was purified using a PCR purification kit (Qiagen), and DNA concentration
705 was determined using a PhiX standard curve. DNA from each sample was pooled at
706 approximately equal input and sequenced on an Illumina NextSeq 500.
707
708 Raw sequencing data was converted to FASTQ files using bcl2fastq2 that were
709 demultiplexed according to ATACseq sample indices corresponding to individual
710 samples. Reads were aligned to GRCh38.
711
712 Chromatin accessibility near transcriptional start sites was analyzed following the
713 standards set forth by the Encode Consortium (Buenrostro et al., 2015). Briefly, scores
714 were obtained by aligning ATAC reads to genome and performing peak calling and next
715 examining peak summit heights at +/- 1kb around the transcriptional start site (TSS) of
716 each gene, then averaging peak scores with a linearly decreasing weight with increasing
717 distance to TSS.
718
719

720 **References**
721

722 Becher, B., Schlitzer, A., Chen, J., Mair, F., Sumatoh, H.R., Teng, K.W.W., Low, D.,
723 Ruedl, C., Riccardi-Castagnoli, P., Poidinger, M., et al. (2014). High-dimensional
724 analysis of the murine myeloid cell system. Nat. Immunol. *15*, 1181–1189.

725 Biswas, S.K., and Mantovani, A. (2010). Macrophage plasticity and interaction with
726 lymphocyte subsets: cancer as a paradigm. Nat. Immunol. *11*, 889–896.

727 Bogdan, C. (2001). Nitric oxide and the immune response. Nat. Immunol. *2*, 907–916.

728 Buenrostro, J., Wu, B., Chang, H., and Greenleaf, W. (2015). ATAC-seq: A Method for
729 Assaying Chromatin Accessibility Genome-Wide. Curr. Protoc. Mol. Biol. Ed. Frederick
730 M Ausubel Al *109*, 21.29.1-21.29.9.

731 Cameron, A.M., Castoldi, A., Sanin, D.E., Flachsmann, L.J., Field, C.S., Puleston, D.J.,
732 Kyle, R.L., Patterson, A.E., Hässler, F., Buescher, J.M., et al. (2019). Inflammatory
733 macrophage dependence on NAD + salvage is a consequence of reactive oxygen
734 species–mediated DNA damage. Nat. Immunol. *20*, 420.

735 Di Gioia, M., Spreafico, R., Springstead, J.R., Mendelson, M.M., Joehanes, R., Levy, D.,
736 and Zanoni, I. (2020). Endogenous oxidized phospholipids reprogram cellular
737 metabolism and boost hyperinflammation. Nat. Immunol. *21*, 42–53.

738 DuPage, M., and Bluestone, J.A. (2016). Harnessing the plasticity of CD4 + T cells to
739 treat immune-mediated disease. Nat. Rev. Immunol. *16*, 149–163.

740 Fleetwood, A.J., Lawrence, T., Hamilton, J.A., and Cook, A.D. (2007). Granulocyte-
741 macrophage colony-stimulating factor (CSF) and macrophage CSF-dependent
742 macrophage phenotypes display differences in cytokine profiles and transcription factor
743 activities: implications for CSF blockade in inflammation. J. Immunol. Baltim. Md 1950
744 *178*, 5245–5252.

745 Gierahn, T.M., Wadsworth Ii, M.H., Hughes, T.K., Bryson, B.D., Butler, A., Satija, R.,
746 Fortune, S., Love, J.C., and Shalek, A.K. (2017). Seq-Well: portable, low-cost RNA
747 sequencing of single cells at high throughput. Nat. Methods *14*, 395–398.

748 Hamilton, J.A. (2019). GM-CSF-Dependent Inflammatory Pathways. Front. Immunol.
749 *10*.

750 Huang, L., Nazarova, E.V., Tan, S., Liu, Y., and Russell, D.G. (2018). Growth of
751 Mycobacterium tuberculosis in vivo segregates with host macrophage metabolism and
752 ontogeny. J. Exp. Med. *215*, 1135–1152.

753 Huynh, J.P., Lin, C.-C., Kimmey, J.M., Jarjour, N.N., Schwarzkopf, E.A., Bradstreet,
754 T.R., Shchukina, I., Shpynov, O., Weaver, C.T., Taneja, R., et al. (2018). Bhlhe40 is an
755 essential repressor of IL-10 during Mycobacterium tuberculosis infection. J. Exp. Med.
756 *215*, 1823–1838.

757 Kasahara, S., Jhingran, A., Dhingra, S., Salem, A., Cramer, R.A., and Hohl, T.M.
758 (2016). Role of Granulocyte-Macrophage Colony-Stimulating Factor Signaling in
759 Regulating Neutrophil Antifungal Activity and the Oxidative Burst During Respiratory
760 Fungal Challenge. J. Infect. Dis. *213*, 1289–1298.

761 Kim, J., D'Annibale, S., Magliozzi, R., Low, T.Y., Jansen, P., Shaltiel, I.A., Mohammed,
762 S., Heck, A.J.R., Medema, R.H., and Guardavaccaro, D. (2014). USP17- and
763 SCFβTrCP-Regulated Degradation of DEC1 Controls the DNA Damage Response. Mol.
764 Cell. Biol. *34*, 4177–4185.

765 Lacey, D.C., Achuthan, A., Fleetwood, A.J., Dinh, H., Roiniotis, J., Scholz, G.M., Chang,
766 M.W., Beckman, S.K., Cook, A.D., and Hamilton, J.A. (2012). Defining GM-CSF– and
767 Macrophage-CSF–Dependent Macrophage Responses by In Vitro Models. J. Immunol.
768 *188*, 5752–5765.

769 Lavin, Y., Winter, D., Blecher-Gonen, R., David, E., Keren-Shaul, H., Merad, M., Jung,
770 S., and Amit, I. (2014). Tissue-Resident Macrophage Enhancer Landscapes Are
771 Shaped by the Local Microenvironment. Cell *159*, 1312–1326.

772 Lawrence, T., and Natoli, G. (2011). Transcriptional regulation of macrophage
773 polarization: enabling diversity with identity. Nat. Rev. Immunol. *11*, 750–761.

774 Lee, S., Kim, S.M., and Lee, R.T. (2013). Thioredoxin and thioredoxin target proteins:
775 from molecular mechanisms to functional significance. Antioxid. Redox Signal. *18*,
776 1165–1207.

777 Liu, S.X., Gustafson, H.H., Jackson, D.L., Pun, S.H., and Trapnell, C. (2020). Trajectory
778 analysis quantifies transcriptional plasticity during macrophage polarization. Sci. Rep.
779 *10*.

780 Liu, Z., Gu, Y., Chakarov, S., Bleriot, C., Kwok, I., Chen, X., Shin, A., Huang, W., Dress,
781 R.J., Dutertre, C.-A., et al. (2019). Fate Mapping via Ms4a3-Expression History Traces
782 Monocyte-Derived Cells. Cell *178*, 1509-1525.e19.

783 Locati, M., Curtale, G., and Mantovani, A. (2020). Diversity, Mechanisms, and
784 Significance of Macrophage Plasticity. Annu. Rev. Pathol. Mech. Dis. *15*, 123–147.

785 Lombardi, M.S., Gilliéron, C., Dietrich, D., and Gabay, C. (2016). SIK inhibition in
786 human myeloid cells modulates TLR and IL-1R signaling and induces an anti-
787 inflammatory phenotype. J. Leukoc. Biol. *99*, 711–721.

788 MacKenzie, K.F., Clark, K., Naqvi, S., McGuire, V.A., Nöehren, G., Kristariyanto, Y.,
789 Bosch, M. van den, Mudaliar, M., McCarthy, P.C., Pattison, M.J., et al. (2013). PGE2
790 Induces Macrophage IL-10 Production and a Regulatory-like Phenotype via a Protein
791 Kinase A–SIK–CRTC3 Pathway. J. Immunol. *190*, 565–577.

792 Macosko, E.Z., Basu, A., Satija, R., Nemesh, J., Shekhar, K., Goldman, M., Tirosh, I.,
793 Bialas, A.R., Kamitaki, N., Martersteck, E.M., et al. (2015). Highly Parallel Genome-wide
794 Expression Profiling of Individual Cells Using Nanoliter Droplets. Cell *161*, 1202–1214.

795 Murray, P.J. (2017). Macrophage Polarization. Annu. Rev. Physiol. *79*, 541–566.

796 Murray, P.J., Allen, J.E., Biswas, S.K., Fisher, E.A., Gilroy, D.W., Goerdt, S., Gordon,
797 S., Hamilton, J.A., Ivashkiv, L.B., Lawrence, T., et al. (2014). Macrophage Activation
798 and Polarization: Nomenclature and Experimental Guidelines. Immunity *41*, 14–20.

799 Natarajan, M., Lin, K.-M., Hsueh, R.C., Sternweis, P.C., and Ranganathan, R. (2006). A
800 global analysis of cross-talk in a mammalian cellular signalling network. Nat. Cell Biol. *8*,
801 571–580.

802 Niemand, C., Nimmesgern, A., Haan, S., Fischer, P., Schaper, F., Rossaint, R.,
803 Heinrich, P.C., and Müller-Newen, G. (2003). Activation of STAT3 by IL-6 and IL-10 in
804 Primary Human Macrophages Is Differentially Modulated by Suppressor of Cytokine
805 Signaling 3. J. Immunol. *170*, 3263–3272.

806 Plugis, N.M., Weng, N., Zhao, Q., Palanski, B.A., Maecker, H.T., Habtezion, A., and
807 Khosla, C. (2018). Interleukin 4 is inactivated via selective disulfide-bond reduction by
808 extracellular thioredoxin. Proc. Natl. Acad. Sci. 201805288.

809 Roussel, M., Ferrell, P.B., Greenplate, A.R., Lhomme, F., Gallou, S.L., Diggins, K.E.,
810 Johnson, D.B., and Irish, J.M. (2017). Mass cytometry deep phenotyping of human
811 mononuclear phagocytes and myeloid-derived suppressor cells from human blood and
812 bone marrow. J. Leukoc. Biol. *102*, 437–447.

813 Sajti, E., Link, V.M., Ouyang, Z., Spann, N.J., Westin, E., Romanoski, C.E., Fonseca,
814 G.J., Prince, L.S., and Glass, C.K. (2020). Transcriptomic and epigenetic mechanisms
815 underlying myeloid diversity in the lung. Nat. Immunol. *21*, 221–231.

816 Salez, L., Singer, M., Balloy, V., Créminon, C., and Chignard, M. (2000). Lack of IL-10
817 synthesis by murine alveolar macrophages upon lipopolysaccharide exposure.
818 Comparison with peritoneal macrophages. J. Leukoc. Biol. *67*, 545–552.

819 Sander, J., Schmidt, S.V., Cirovic, B., McGovern, N., Papantonopoulou, O., Hardt, A.-L.,
820 Aschenbrenner, A.C., Kreer, C., Quast, T., Xu, A.M., et al. (2017). Cellular
821 Differentiation of Human Monocytes Is Regulated by Time-Dependent Interleukin-4
822 Signaling and the Transcriptional Regulator NCOR2. Immunity *47*, 1051-1066.e12.

823 Sanin, D.E., Matsushita, M., Klein Geltink, R.I., Grzes, K.M., van Teijlingen Bakker, N.,
824 Corrado, M., Kabat, A.M., Buck, M.D., Qiu, J., Lawless, S.J., et al. (2018). Mitochondrial
825 Membrane Potential Regulates Nuclear Gene Expression in Macrophages Exposed to
826 Prostaglandin E2. Immunity *49*, 1021-1033.e6.

827 Schneemann, M., and Schoedon, G. (2002). Species differences in macrophage NO
828 production are important. Nat. Immunol. *3*, 102–102.

829 Schulz, D., Severin, Y., Zanotelli, V.R.T., and Bodenmiller, B. (2019). In-Depth
830 Characterization of Monocyte-Derived Macrophages using a Mass Cytometry-Based
831 Phagocytosis Assay. Sci. Rep. *9*, 1–12.

832 Spath, S., Komuczki, J., Hermann, M., Pelczar, P., Mair, F., Schreiner, B., and Becher,
833 B. (2017). Dysregulation of the Cytokine GM-CSF Induces Spontaneous Phagocyte
834 Invasion and Immunopathology in the Central Nervous System. Immunity *46*, 245–260.

835 Subramanian Vignesh, K., Landero Figueroa, J.A., Porollo, A., Caruso, J.A., and
836 Deepe, G.S. (2013). Granulocyte Macrophage-Colony Stimulating Factor Induced Zn
837 Sequestration Enhances Macrophage Superoxide and Limits Intracellular Pathogen
838 Survival. Immunity *39*, 697–710.

839 Van den Bossche, J., Baardman, J., Otto, N.A., van der Velden, S., Neele, A.E.,
840 van den Berg, S.M., Luque-Martin, R., Chen, H.-J., Boshuizen, M.C.S., Ahmed, M., et
841 al. (2016). Mitochondrial Dysfunction Prevents Repolarization of Inflammatory
842 Macrophages. Cell Rep. *17*, 684–696.

843 Wang, Y., Ji, N., Gong, X., Ni, S., Xu, L., and Zhang, H. (2020). Thioredoxin-1
844 attenuates atherosclerosis development through inhibiting NLRP3 inflammasome.
845 Endocrine.

846 Werz, O., Gerstmeier, J., Libreros, S., Rosa, X.D. la, Werner, M., Norris, P.C., Chiang,
847 N., and Serhan, C.N. (2018). Human macrophages differentially produce specific
848 resolvin or leukotriene signals that depend on bacterial pathogenicity. Nat. Commun. *9*,
849 1–12.

850 West, A.P., Brodsky, I.E., Rahner, C., Woo, D.K., Erdjument-Bromage, H., Tempst, P.,
851 Walsh, M.C., Choi, Y., Shadel, G.S., and Ghosh, S. (2011). TLR signalling augments
852 macrophage bactericidal activity through mitochondrial ROS. Nature *472*, 476–480.

853 Xue, J., Schmidt, S.V., Sander, J., Draffehn, A., Krebs, W., Quester, I., De Nardo, D.,
854 Gohel, T.D., Emde, M., Schmidleithner, L., et al. (2014). Transcriptome-Based Network
855 Analysis Reveals a Spectrum Model of Human Macrophage Activation. Immunity *40*,
856 274–288.

857

858

Acknowledgments

This work was supported by MIT Biological Engineering (BDB), The Ragon Institute of MGH, MIT, and Harvard (AKS, BDB, SMF), NIH CFAR P30 AI060354, The Bill and Melinda Gates Foundation (AKS, SMF), NIH R01 AI123286 (SMF), NIH T32AI132120-01 (GHB), NIH R01 AI12328 (SMF, GHB), NIH R01 GM081871 (BLH, BB)Searle Scholars Program (AKS), Beckman Young Investigator Program (AKS), Pew-Stewart Scholars Program for Cancer Research (AKS), and the Sloan Fellowship in Chemistry (AKS) . CYI was funded by an HHMI Medical Research Fellowship. CG is supported by an NSF Graduate Research Fellowship. B.H. is supported by the Department of Defense (DoD) through the National Defense Science and Engineering Graduate Fellowship (NDSEG).

Author Information

Contributions

CYI, CG, GHB, AN, NAA, MHW, TKH, SLS, BH, BB, AKS, SMF, and BDB conceived and performed experiments. CYI, CG, GHB, AN, NAA, MHW, TKH, SLS, BH, BB, AKS, SMF, and BDB all performed data analysis. All authors contributed to writing of the manuscript and analysis of experimental results.

Competing Interests

A.K.S. reports compensation for consulting and/or SAB membership from Merck, Honeycomb Biotechnologies, Cellarity, Repertoire Immune Medicines, Orche Bio, and Dahlia Biosciences.

Figure Legends

Figure 1: Multi-dimensional profiling of human monocyte-derived macrophages identifies differentiation and activation-mediated phenotypes.

(A) Methodological workflow for generation of macrophage libraries from CD14+ monocytes from healthy donors. Monocytes were differentiated with M-CSF or GM-CSF for 3 days (differentiation only phase) prior to the addition of additional ligands (PBS, LPS, IFN-γ, IL-4, IL-6, and IL-10) for an additional 3 days (activation phase). After 3 days in the activation phase, macrophages were washed with PBS, detached, counted, and re-plated equally to characterize macrophage phenotype.

(B) Analysis of macrophage surface marker expression using a digital gating strategy to identify the percentage of macrophages expressing a given marker (MO-MCSF cells). Representative of 3 donors.

(C) Analysis of macrophage surface marker expression using an analog quantification strategy (mean fluorescence intensity, MFI) to quantify the abundance of a given marker on the macrophage surface (MO-MCSF cells). Representative of 3 donors.

(D) Quantification of CD274 across multiple donors reveals upregulation of CD274 following IFN-γ or LPS stimulation (MO-MCSF cells). Each colored line is an individual donor. Comparisons made using a ratio paired t test. (*, $p < 0.05$).

(E) Z-score of cytokine secretion screen in MO-MCSF or MO-GMCSF cells stimulated with media, 100 ng/mL LPS or 100 ng/mL Pam3Csk4 (P3C).

(F) Secretion of IL-10 across all 12 macrophage populations following 100 ng/mL LPS or 100 ng/mL P3C stimulation. (****, $p < 0.0001$, ***, $p < 0.001$, **, $p < 0.01$, ns = not significant). Representative of 3 donors.

(G) Secretion of TNFα across all 6 MO-GMCSF populations following 100 ng/L LPS or 100 ng/mL P3C stimulation. (****, $p < 0.0001$, ***, $p < 0.001$, **, $p < 0.01$, *, $p <0.05$, ns = not significant). Representative of 3 donors.

(H) Phosphorylation of STAT3 in MO-GMCSF cells following IL-10 stimulation.

Figure 2: Single cell RNA sequencing reveals characteristics of macrophage state.

(A) Log-normalized expression of canonical marker genes in 1,742 MO-GMCSF and 4,803 MO-MCSF from 2 donors (N = 399 MO-GMCSF- and 1,941 MO-M-CSF donor 1; 1,343 MO-GMCSF- and 2,862 MO-MCSF-treated cells, donor 2). Center line, median; box limits, first and third quartile; whiskers, +/- 1.5 interquartile range; dots, individual cells. G = MO-GMCSF-treated cells; M = MO-MCSF-treated cells.

933 (B) Standard scaled expression of marker genes identified in 250 randomly subsampled
934 cells from each donor and condition. M_A = M-CSF-treated, donor A; M_B = M-CSF-treated,
935 donor 2; G_A = GM-CSF-treated, donor A; G_B = GM-CSF-treated, donor B.
936
937 (C) Log-normalized expression of top marker genes identified in (B) across all cells. (AUC,
938 TXN: 0.845, ALOX5AP: 0.808, CHI3L1: 0.222, MGLL: 0.225)
939
940 (D) Significantly enriched gene ontology terms in marker gene set for MO-GMCSF- cells
941 (left) and M-CSF-treated cells (right), determined by hypergeometric test after filtering by
942 semantic similarity (Benjamini-Hochberg-corrected p-value < 0.05; semantic similarity
943 threshold = 0.5). GO term enrichment in the marker set was calculated relative to
944 enrichment in the background set of genes captured in all sequencing runs with >100
945 total counts across runs.
946
947 Western blotting of cell lysates treated with 50 ng/mL M-CSF, 50 ng/mL GM-CSF, or 10
948 ng/mL each of IFN-γ and LPS (Y+L) for 24 h for thioredoxin (E) and 5-lipoxygenase (F).
949 Beta-actin was used as a loading control. Representative of 4 donors.
950
951 (G) Analysis of CD36 expression by flow cytometry in MO-MCSF or MO-GMCSF cells.
952 Representative of 3 donors.
953
954 (H) Analysis of CD206 expression by flow cytometry in MO-MCSF or MO-GMCSF cells.
955 Representative of 3 donors.
956
957 **Figure 3: Combinatorial treatment of monocytes or MO-MCSF or MO-GMCSF cells**
958 **with GM-CSF or M-CSF reveals unexpected features of the GM-CSF-IL-10 circuit.**
959
960 (A) Analysis of GM-CSF (CD116) or M-CSF (CD115) receptor surface expression by flow
961 cytometry in MO-MCSF or MO-GMCSF cells. Representative of 3 donors.
962
963 (B) Design of IL-10 phenotypic stability experiment in MO-MCSF or MO-GMCSF cells.
964
965 (C) Secretion of IL-10 across polarized or repolarized MO-MCSF and MO-GMCSF cells
966 following 100 ng/mL LPS stimulation. (****, p < 0.0001, ***, p < 0.001, **, p < 0.01, ns =
967 not significant). Representative of 3 donors.
968
969 (D) Design of GM-CSF/M-CSF titration checkerboard experiment.
970
971 (E) Secretion of IL-10 across monocytes differentiated with various combinations of GM-
972 CSF or M-CSF following 100 ng/mL LPS stimulation. Representative of 3 donors.
973
974 **Figure 4: Interference with inducible nitric oxide synthase or salt-inducible kinase**
975 **activity does not enhance IL-10 production while scavenging oxidative radicals**
976 **with N-acetylcysteine in MO-GMCSF cells does.**
977

(A) Secretion of IL-10 in MO-GMCSF or MO-MCSF cells following incubation with 1400W, an iNOS inhibitor, and treatment with 100 ng/mL LPS stimulation. (****, $p < 0.0001$, ns = not significant). Representative of 3 donors.

(B) Secretion of IL-10 in MO-MCSF cells following incubation with HG-9-91-01, a salt-inducible kinase inhibitor, and treatment with 100 ng/mL LPS stimulation. (****, $p < 0.0001$, ***, $p < 0.001$, **, $p < 0.01$). Representative of 3 donors.

(C) Secretion of IL-10 in MO-GMCSF cells that were pre-treated with 100 nM trichostatin-A (TSA) or vehicle control prior to 6-day differentiation and next stimulated with 100 ng/mL LPS for 16 hours. (****, $p < 0.0001$, ns = not significant). Representative of 2 donors.

(D) Log-normalized expression of genes associated with oxidative signaling in MO-MCSF or MO-GMCSF cells.

(E) Secretion of IL-10 in MO-GMCSF or MO-MCSF cells that were pre-treated with 5 mM N-acetylcysteine prior to 6-day differentiation and next stimulated 100 ng/mL LPS for 16 hours. (***, $p < 0.001$, *, $p <0.05$, ns = not significant). Representative of 3 donors.

Supplemental Figure Legends

Supplemental Figure 1: Analysis of macrophage surface marker expression using a digital gating strategy to identify the percentage of macrophages expressing a given marker (MO-GMCSF cells). Representative of 2 donors.

Supplemental Figure 2: Analysis of macrophage surface marker expression using an analog quantification strategy (mean fluorescence intensity, MFI) to quantify the abundance of a given marker on the macrophage surface (MO-GMCSF cells). Representative of 2 donors.

Supplemental Figure 3: Quantification of CD274 across multiple donors reveals upregulation of CD274 following IFN-γ or LPS stimulation (MO-GMCSF cells). Each colored line is an individual donor.

Supplemental Figure 4: Analysis of IL-10 production in MO-MCSF cells following LPS stimulation using intracellular cytokine staining and flow cytometry. Production of IL-10 following 100 ng/mL LPS stimulation was monitored using intracellular cytokine staining.

Supplemental Figure 5: Read mapping quality in samples. Violin plots depict number of transcripts (A), genes (B), and percentage of reads aligning to mitochondrial genes (C), separated by GM-CSF and M-CSF treatment and donor.

Supplemental Table 1: Differential expression of all genes captured in scRNAseq analysis of MO-GMCSF and MO-MCSF cells. The AUC column presents the results of the area under the curve analysis used to identify marker genes for MO-GMCSF and MO-MCSF cells. The avg_log2FC column presents the log2(fold change) in gene expression for MO-GMCSF cells relative to MO-MCSF cells. The power column represents the classification power of a particular gene. The pct.g column indicates the percentage of MO-GMCSF cells expressing a particular gene. The pct.m column indicates the percentage of MO-MCSF cells expressing a particular gene. The p_val column represents the p-value of differential gene expression between MO-GMCSF and MO-MCSF cells as determined by Wilcoxon rank sums test. The p_val_adj column represents the p-value of differential gene expression between MO-GMCSF and MO-MCSF cells following Benjamini-Hochberg correction.

Supplemental Table 2: Gene ontology analysis of marker genes from analysis of MO-GMCSF and MO-MCSF cells by scRNAseq. The ID column represents the ID of the gene ontology term. The Description column describes and summarizes the gene ontology term. The GeneRatio column captures the number of significant marker genes belonging to a particular gene ontology category out of all the significant marker genes for MO-GMCSF or MO-MCSF cells. The BgRatio column captures the number of captured genes belonging to a particular gene ontology category out of all captured genes for MO-GMCSF or MO-MCSF cells. The background set of genes was constructed by identifying genes captured in all sequencing runs with >100 total counts across runs. The

pvalue column captures the results of the hypergeometric test. The p.adjust column is after filtering gene ontology terms by semantic similarity (Benjamini-Hochberg-corrected p-value < 0.05; semantic similarity threshold = 0.5). The qvalue column was determined using a false-discovery rate approach. The geneID column captures the gene names of those genes belonging to the particular Gene Ontology term. The Count column enumerates the number of significant marker genes falling into a particular Gene Ontology category.

Supplemental Table 3: Chromatin accessibility scores of MO-MCSF and MO-GMCSF cells. The Gene column represents the gene ID. The GM-CSF Score column summarizes the chromatin accessibility scores for all 6 MO-GMCSF ATACseq samples. The M-CSF Score column summarizes the chromatin accessibility scores for all 6 MO-MCSF ATACseq samples. The Mean GM-CSF Score column presents the mean chromatin accessibility score for all 6 MO-GMCSF samples. The Mean GM-CSF Score column presents the mean chromatin accessibility score for all 6 MO-GMCSF samples. The Mean M-CSF Score column presents the mean chromatin accessibility score for all 6 MO-MCSF samples. The Uncorrected p-value column is the result of a t-test for each gene.

Figure 1

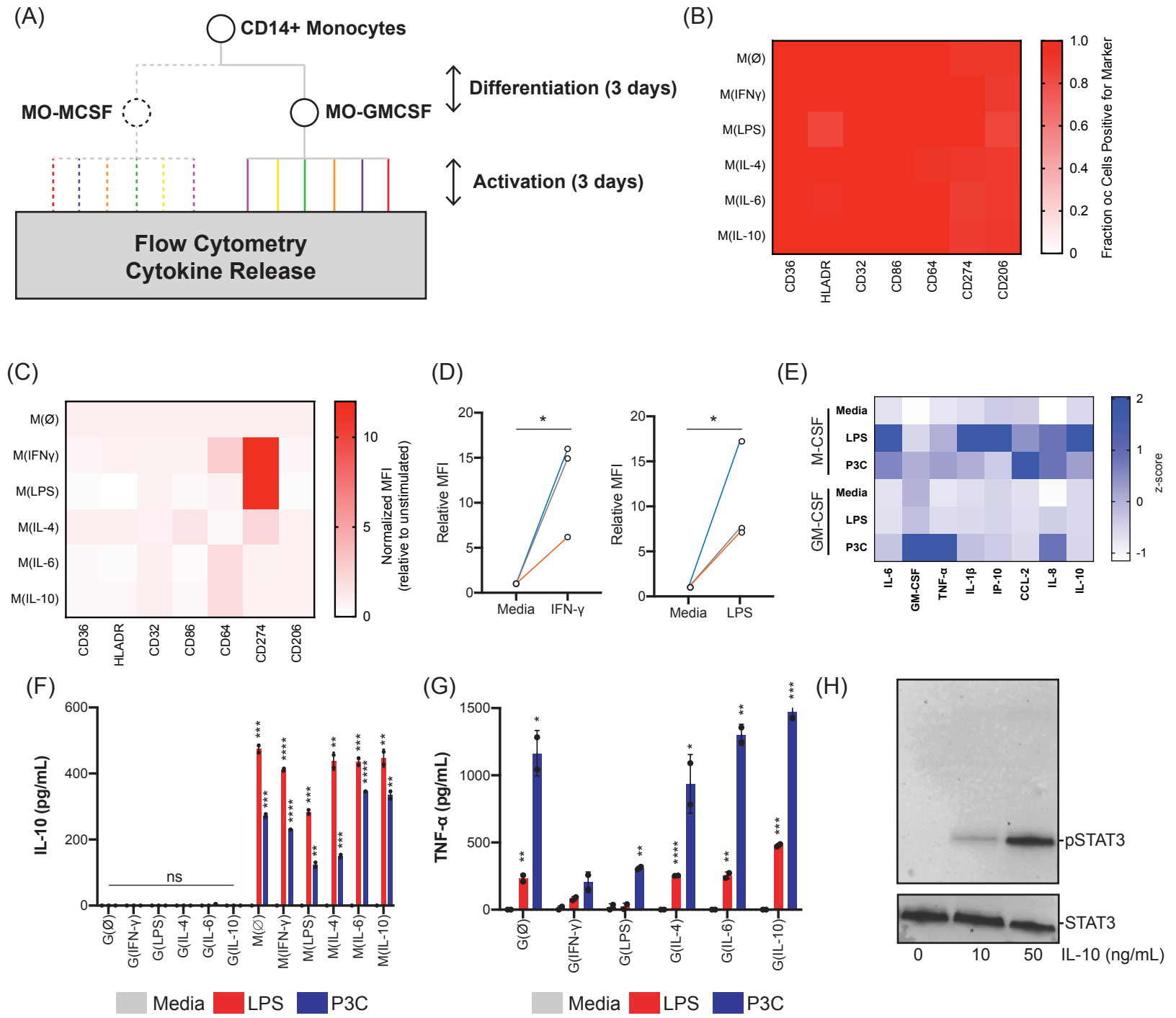
(A)
CD14+ Monocytes
MO-MCSF
MO-GMCSF
Differentiation (3 days)
Activation (3 days)
Flow Cytometry
Cytokine Release
(B)
M(Ø)
M(IFNγ)
M(LPS)
M(IL-4)
M(IL-6)
M(IL-10)
CD36
HLADR
CD32
CD86
CD64
CD274
CD206
Fraction oc Cells Positive for Marker
(C)
Normalized MFI
(relative to unstimulated)
(D)
Relative MFI
Media
IFN-γ
LPS
(E)
M-CSF
GM-CSF
Media
LPS
P3C
IL-6
GM-CSF
TNF-α
IL-1β
IP-10
CCL-2
IL-8
IL-10
z-score
(F)
IL-10 (pg/mL)
ns
G(Ø)
G(IFN-γ)
G(LPS)
G(IL-4)
G(IL-6)
G(IL-10)
M(Ø)
M(IFN-γ)
M(LPS)
M(IL-4)
M(IL-6)
M(IL-10)
Media
LPS
P3C
(G)
TNF-α (pg/mL)
Media
LPS
P3C
(H)
pSTAT3
STAT3
0
10
50
IL-10 (ng/mL)

Figure 2

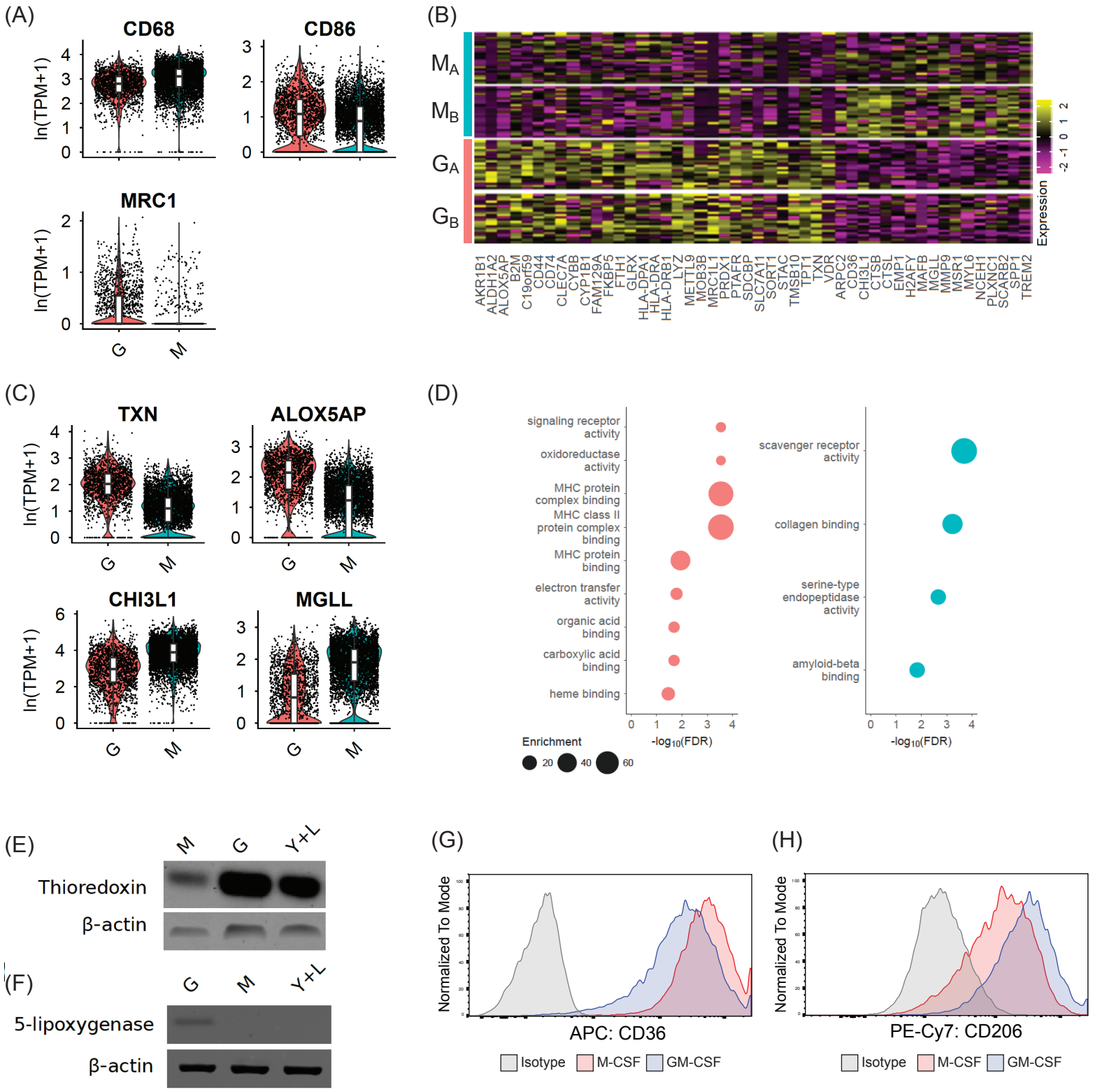
(A)
CD68
CD86
MRC1
ln(TPM+1)
G
M
(B)
M_A
M_B
G_A
G_B
Expression
AKR1B1
ALDH1A2
ALOX5AP
B2M
C19orf59
CD44
CD74
CLEC7A
CYBB
CYP1B1
FAM129A
FKBP5
FTH1
GLRX
HLA-DPA1
HLA-DRA
HLA-DRB1
LYZ
METTL9
MOB3B
MRC1L1
PRDX1
PTAFR
SDCBP
SLC7A11
SORT1
STAC
TMSB10
TPT1
TXN
VDR
ARPC2
CD36
CHI3L1
CTSB
CTSL
EMP1
H2AFY
MAFB
MGLL
MMP9
MSR1
MYL6
NCEH1
PLXNC1
SCARB2
SPP1
TREM2
(C)
TXN
ALOX5AP
CHI3L1
MGLL
ln(TPM+1)
G
M
(D)
signaling receptor activity
oxidoreductase activity
MHC protein complex binding
MHC class II protein complex binding
MHC protein binding
electron transfer activity
organic acid binding
carboxylic acid binding
heme binding
scavenger receptor activity
collagen binding
serine-type endopeptidase activity
amyloid-beta binding
$-\log_{10}$(FDR)
Enrichment
20
40
60
(E)
M
G
Y+L
Thioredoxin
β-actin
(F)
G
M
Y+L
5-lipoxygenase
β-actin
(G)
Normalized To Mode
APC: CD36
Isotype
M-CSF
GM-CSF
(H)
Normalized To Mode
PE-Cy7: CD206
Isotype
M-CSF
GM-CSF

Figure 3

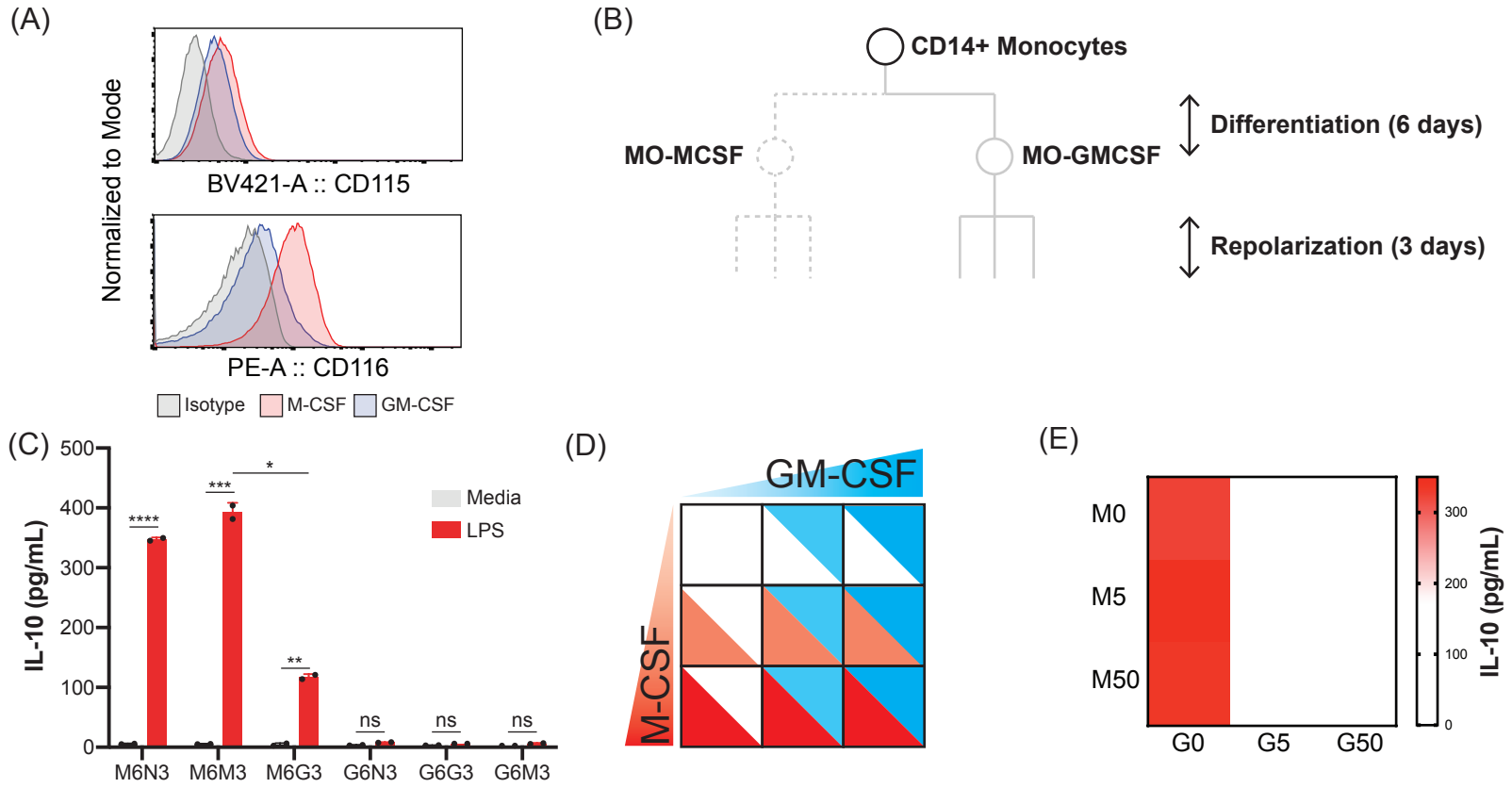
(A)
Normalized to Mode
BV421-A :: CD115
PE-A :: CD116
Isotype
M-CSF
GM-CSF
(B)
CD14+ Monocytes
MO-MCSF
MO-GMCSF
Differentiation (6 days)
Repolarization (3 days)
(C)
IL-10 (pg/mL)
500
400
300
200
100
0
****
***
*
**
ns
ns
ns
Media
LPS
M6N3
M6M3
M6G3
G6N3
G6G3
G6M3
(D)
GM-CSF
M-CSF
(E)
M0
M5
M50
G0
G5
G50
300
200
100
0
IL-10 (pg/mL)

Figure 4

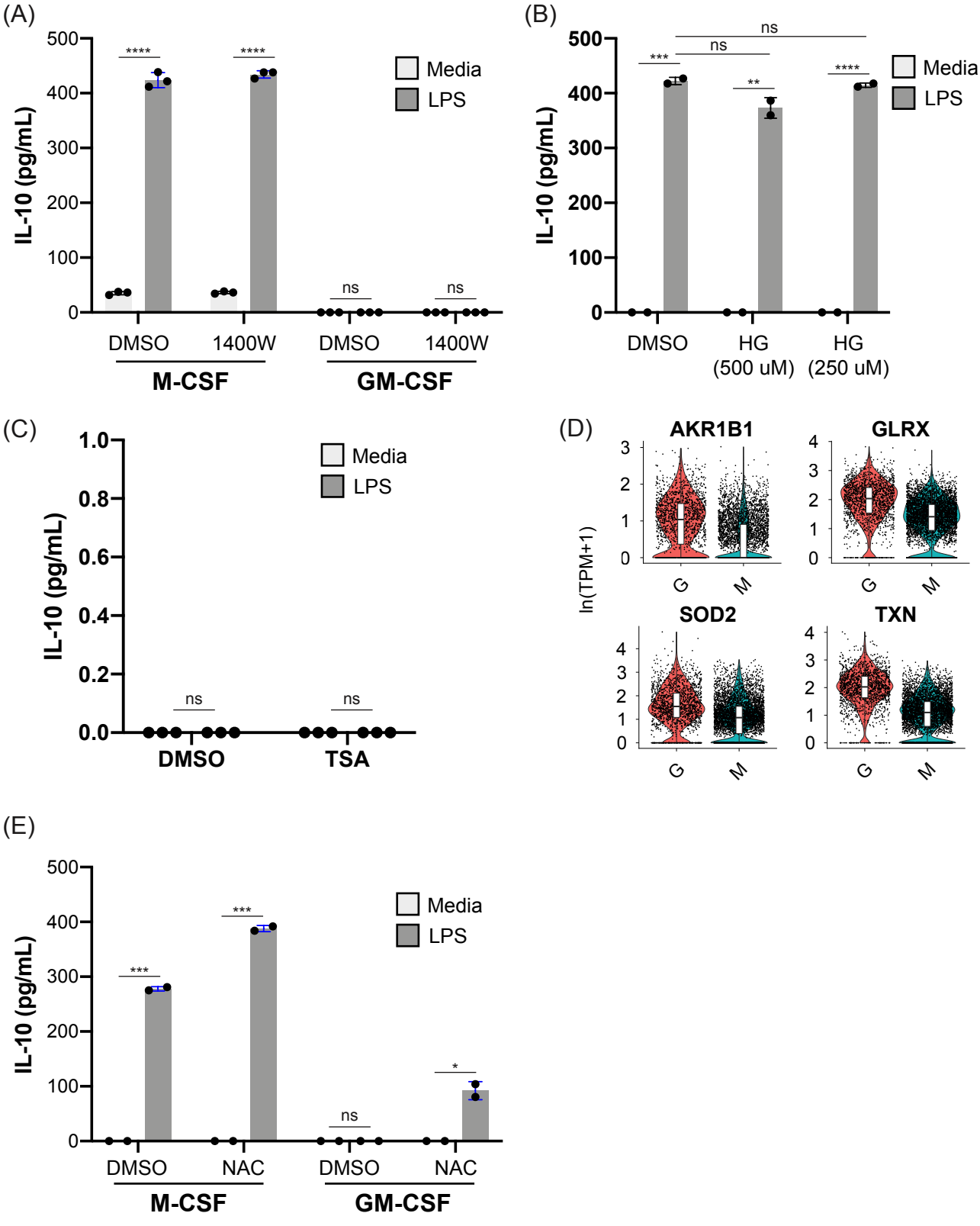
(A)
IL-10 (pg/mL)
500
400
300
200
100
0
****
****
ns
ns
Media
LPS
DMSO
1400W
DMSO
1400W
M-CSF
GM-CSF
(B)
IL-10 (pg/mL)
500
400
300
200
100
0
ns
ns
***
**
****
Media
LPS
DMSO
HG (500 uM)
HG (250 uM)
(C)
IL-10 (pg/mL)
1.0
0.8
0.6
0.4
0.2
0.0
Media
LPS
ns
ns
DMSO
TSA
(D)
ln(TPM+1)
AKR1B1
GLRX
SOD2
TXN
G
M
(E)
IL-10 (pg/mL)
500
400
300
200
100
0
***
***
ns
*
Media
LPS
DMSO
NAC
DMSO
NAC
M-CSF
GM-CSF

Figure 2

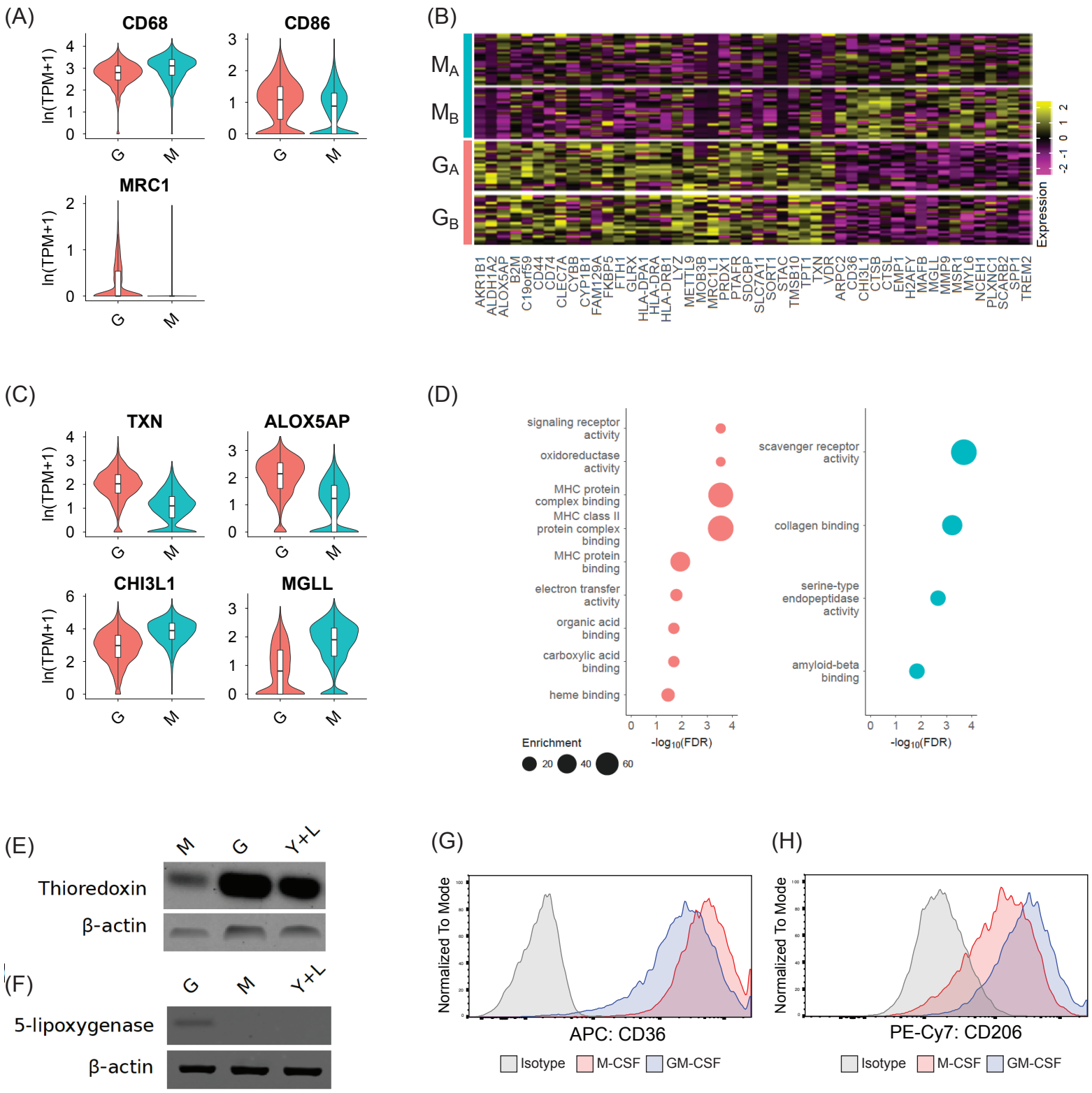
(A)
CD68
CD86
MRC1
ln(TPM+1)
G
M
(B)
M_A
M_B
G_A
G_B
Expression
AKR1B1
ALDH1A2
ALOX5AP
B2M
C19orf59
CD44
CD74
CLEC7A
CYBB
CYP1B1
FAM129A
FKBP5
FTH1
GLRX
HLA-DPA1
HLA-DRA
HLA-DRB1
LYZ
METTL9
MOB3B
MRC1L1
PRDX1
PTAFR
SDCBP
SLC7A11
SORT1
STAC
TMSB10
TPT1
TXN
VDR
ARPC2
CD36
CHI3L1
CTSB
CTSL
EMP1
H2AFY
MAFB
MGLL
MMP9
MSR1
MYL6
NCEH1
PLXNC1
SCARB2
SPP1
TREM2
(C)
TXN
ALOX5AP
CHI3L1
MGLL
ln(TPM+1)
G
M
(D)
signaling receptor activity
oxidoreductase activity
MHC protein complex binding
MHC class II protein complex binding
MHC protein binding
electron transfer activity
organic acid binding
carboxylic acid binding
heme binding
scavenger receptor activity
collagen binding
serine-type endopeptidase activity
amyloid-beta binding
$-\log_{10}$(FDR)
Enrichment
20
40
60
(E)
M
G
Y+L
Thioredoxin
β-actin
(F)
G
M
Y+L
5-lipoxygenase
β-actin
(G)
Normalized To Mode
APC: CD36
Isotype
M-CSF
GM-CSF
(H)
Normalized To Mode
PE-Cy7: CD206
Isotype
M-CSF
GM-CSF

Figure 3

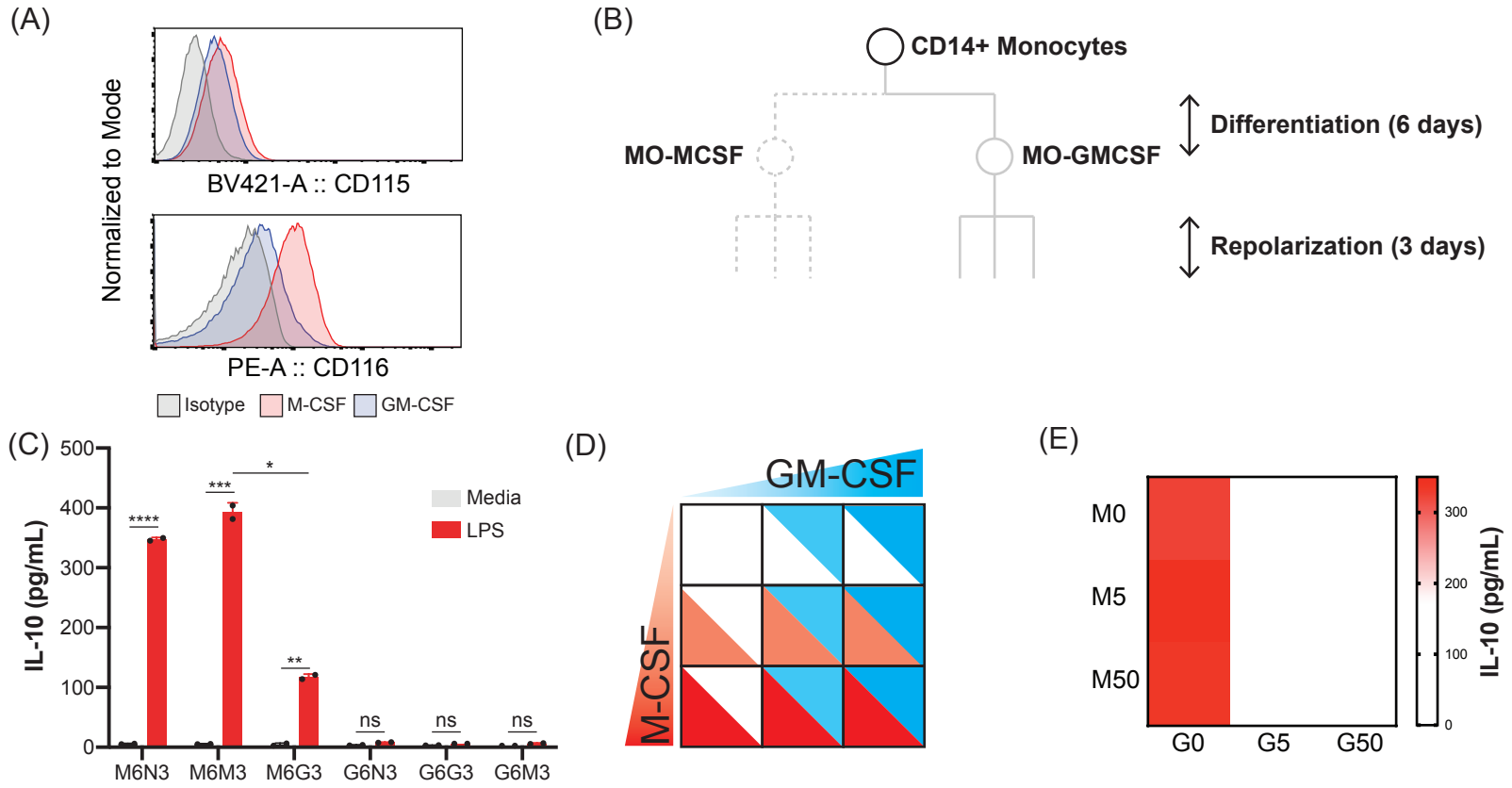
(A)
Normalized to Mode
BV421-A :: CD115
PE-A :: CD116
Isotype
M-CSF
GM-CSF
(B)
CD14+ Monocytes
MO-MCSF
MO-GMCSF
Differentiation (6 days)
Repolarization (3 days)
(C)
IL-10 (pg/mL)
500
400
300
200
100
0
****
***
*
**
ns
ns
ns
Media
LPS
M6N3
M6M3
M6G3
G6N3
G6G3
G6M3
(D)
GM-CSF
M-CSF
(E)
M0
M5
M50
G0
G5
G50
300
200
100
0
IL-10 (pg/mL)

Figure 4

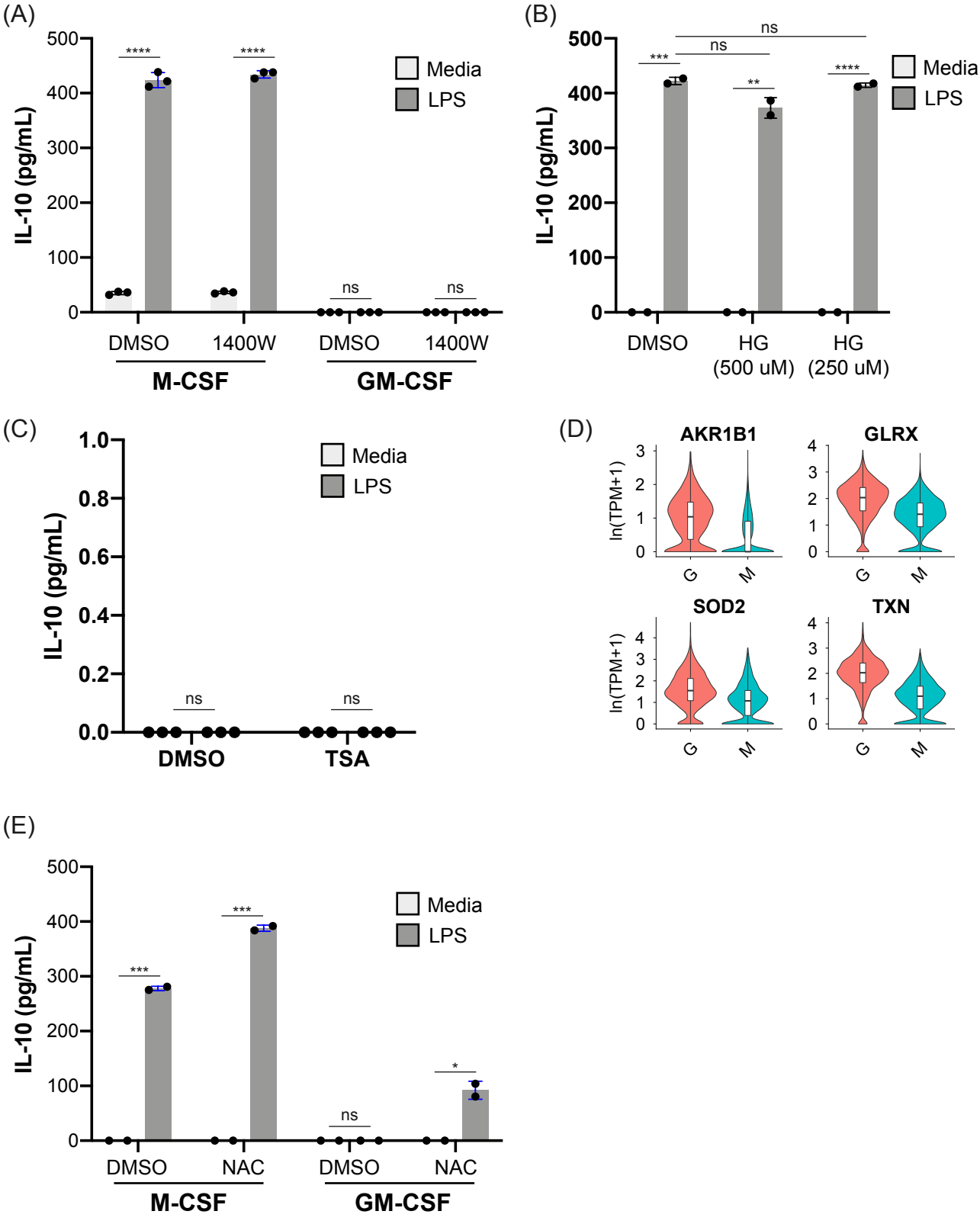
(A)
IL-10 (pg/mL)
500
400
300
200
100
0
****
****
ns
ns
Media
LPS
DMSO
1400W
DMSO
1400W
M-CSF
GM-CSF
(B)
IL-10 (pg/mL)
500
400
300
200
100
0
ns
ns
***
**
****
Media
LPS
DMSO
HG (500 uM)
HG (250 uM)
(C)
IL-10 (pg/mL)
1.0
0.8
0.6
0.4
0.2
0.0
Media
LPS
ns
ns
DMSO
TSA
(D)
AKR1B1
GLRX
SOD2
TXN
ln(TPM+1)
G
M
(E)
IL-10 (pg/mL)
500
400
300
200
100
0
***
***
ns
*
Media
LPS
DMSO
NAC
DMSO
NAC
M-CSF
GM-CSF